THERMODYNAMICS OF DEHYDRATION AND HYDRATION IN NATROLITE AND ANALCIME

By

JIE WANG

A THESIS PRESENTED TO THE GRADUATE SCHOOL
OF THE UNIVERSITY OF FLORIDA IN PARTIAL FULFILLMENT
OF THE REQUIREMENTS FOR THE DEGREE OF
MASTER OF SCIENCE

UNIVERSITY OF FLORIDA

2006

ACKNOWLEDGMENTS

Funding for this project was provided by an NSF-EAR grant to Dr. Philip Neuhoff at the University of Florida. First, I gratefully acknowledge Dr. Neuhoff for his support during the past two years in my study and living in United States. His patience and advice helped me overcome a lot of difficulties and finally finish this project. I would like to thank my committee (Dr. Mike Perfit and Dr. Jon Martin) and Dr. Guerry McClellan for their support and guidance. I would also like to thank Laura Ruhl and Scott Keddy for their assistance with sample preparation, Jane Gustavson and Gokce Atalan for their help in my research. Special thanks also go to Ryan Francis, Shawn Malone, Susanna Blair, Derrick Newkirk and all my other friends for their help with my spoken and written English. Finally, I would like to thank my parents for all their love and support throughout my life.

TABLE OF CONTENTS

LIST OF TABLES

LIST OF FIGURES

Abstract of Thesis Presented to the Graduate School
of the University of Florida in Partial Fulfillment of the
Requirements for the Degree of Master of Science

THERMODYNAMICS OF DEHYDRATION AND HYDRATION
IN NATROLITE AND ANALCIME

By

Jie Wang

August 2006

Chair: Philip S. Neuhoff
Major Department: Geological Sciences

Zeolites are framework aluminosilicates with open channels containing molecular water and extra-framework cations. Their distinctive crystal structures endow them with high cation-exchange capacities and molecular sieve capabilities, which are widely applied in water softening, catalysis and wastewater treatment. Thermodynamic data are essential to determine the stability of zeolites and evaluate their paragenesis.

Reversible dehydration of intracrystalline water in zeolites is an important consideration for assessing their stability, particularly at elevated temperatures and pressures. Derivation of thermodynamic properties of dehydration and rehydration from phase equilibria requires prior knowledge of the heat capacity of hydration ($\Delta C_{p,r}$) in order to reduce the number of unknown variables. However, experimental determination of $\Delta C_{p,r}$ is difficult because measurements at elevated temperature often contain contributions from the enthalpy of dehydration. Statistical-mechanical reasoning is often used to suggest that $\Delta C_{p,r}$ is independent of temperature, permitting application of $\Delta C_{p,r}$

determined at relatively low temperatures where dehydration is not an issue. We focused our study on natrolite ($Na_2Al_2Si_3O_{10}\cdot 2H_2O$) and analcime ($NaAlSi_2O_6\cdot H_2O$), two common rock-forming zeolites that are chemically and structurally less complex than other zeolites due to the presence of only one extraframework cation (Na^+) and one crystallographically-distinct water site. In this study, we have directly measured heat capacities (C_p) of hydrated and dehydrated zeolites by the simultaneous differential scanning calorimetric (DSC) and thermogravimetric analysis (TGA) system. The temperature dependence of enthalpies of hydration (ΔH_{hyd}) in analcime and natrolite was determined by the newly developed isothermal immersion technique. The temperature dependence of ΔH_{hyd} provides an alternative means of assessing $\Delta C_{p,r}$.

The results obtained by these approaches show that the behaviors of $\Delta C_{p,r}$ are different for different zeolites. In natrolite, $\Delta C_{p,r}$ determined from ΔH_{hyd} between 373 and 473 K is independent of temperature, but is substantially larger than determined by direct measurements of C_p. This implies the presence of an excess heat capacity of mixing due to the solvus behavior of natrolite in solid solution. In the case of analcime, the situation is more complicated. In the lower temperature range (< 463 K), $\Delta C_{p,r}$, determined from ΔH_{hyd}, is relatively insensitive to the temperature and in agreement with direct C_p measurements, whereas in the higher temperature range (> 463 K), $\Delta C_{p,r}$ decreases and increases rapidly with increasing temperature, indicating a phase transition. Coupled determination of ΔH_{hyd} and $\Delta C_{p,r}$ as a function of temperature provides important and fundamental insights into the thermodynamics of dehydration and rehydration in zeolites, and should aid quantitative prediction of the water content of zeolites as a function of temperature, pressure, and the chemical potential of H_2O in geologic systems.

CHAPTER 1
INTRODUCTION

Minerals that contain molecular water within their structures are modally-important at and near the earth's surface. These mineral hydrates (e.g., oxyhydroxides, sulfates, carbonates, clay minerals, zeolites) are important reservoirs for water in earth's crust. Many of these phases are also important naturally-occurring nanomaterials (e.g., Banfield and Zhang, 2001). A common feature of some hydrate minerals is the ability to reversibly dehydrate in response to changes in temperature, pressure, and the chemical potential of H_2O, a process that has significant implications for assessing the water content of the crust and the stability of the minerals themselves (e.g., Bish and Carey, 2001). Therefore, the stability and chemical behavior of hydrates are critical considerations for assessing the behavior of low-temperature geochemical systems. This study focuses on zeolites, which, in addition to being geologically important phases in low temperature environments (e.g., Coombs et al., 1959; Hay and Sheppard, 2001; Neuhoff et al., 2000), serve as important model systems for the study of dehydration by mineral hydrates because they have well-delineated crystal structures (e.g., Armbruster and Gunter, 2001; Meier et al., 2001) and are readily manipulated experimentally (e.g., Bish and Carey, 2001).

Understanding the formation and stability of zeolites in geologic systems is limited in part by an insufficient understanding of the dehydration behavior of these minerals. Partial dehydration (i.e., compositional changes) during calorimetric or phase equilibrium experiments complicates derivation of thermodynamic properties for these minerals (e.g.,

Carey, 1993; Helgeson et al., 1978). Thus, developing experimental techniques that provide for quantitative assessment of the thermodynamic consequences of partial dehydration is critical for evaluating zeolites stability relations. In addition, the stability of zeolites with respect to other aluminosilicates is dependent on their hydration state as hydrated zeolites are often stable at earth surface conditions with respect to dense aluminosilicate assemblages and free water, but their dehydrated equivalents are not (e.g., Shim et al. 1999). In fact, accurate prediction of the partial dehydration of zeolites can be key to understanding their stability in geologic environments (e.g., Neuhoff and Bird, 2001). Dehydration also has a dramatic effect on the ion exchange properties of zeolites (Fridriksson et al., 1999; Bish and Carey, 2001). Complicating the thermodynamic description of these processes is the fact that many zeolites contain multiple, energetically distinct water sites (Fridriksson et al., 2003; Fialips et al., 2005).

This study applies new experimental techniques for assessing the thermodynamic properties of dehydration reactions in zeolites, focusing on the natural zeolites analcime and natrolite. Through detailed laboratory analysis this study attempts to answer three specific questions:

1. Are the heat capacities of dehydration reactions in zeolites invariant with respect to temperature, as previously suggested?
2. Do experimental measurements of the bulk heat capacities of hydrated and dehydrated zeolites permit accurate assessment of the temperature dependence of the heat of dehydration determined calorimetrically or through equilibrium observations?
3. What are the water contents of analcime and natrolite in the geologic settings in which they occur?

In the pages to follow, we comment on problems in four chapters. Chapter 1 (this chapter) provides background material relevant to this study. Chapter 2 presents

experimental determinations of the temperature dependence of the heat of hydration and heat capacity of hydration in analcime. Chapter 3 is a similar study of natrolite. Chapter 4 compares the results for analcime and natrolite and discusses the broader implication of this study.

Background Studies

Mineralogical Nature of Zeolites

Zeolites are framework aluminosilicates whose structure is characterized by a framework of Si- and Al-centered tetrahedra arranged to form 2-10 Å channels that contain water molecules and extraframework (charge-balancing) cations (Gottardi and Galli, 1985). The general chemical formula for natural zeolites is

$(Li, Na, K)_a(Mg, Ca, Sr, Ba)_d[Al_{(a+2d)}Si_{n-(a+2d)}O_{2n}]\cdot mH_2O$

where the portion in square brackets represents the framework and rest of the species reside within the channels (e.g., Gottardi and Galli, 1985). While modification of the framework composition requires dissolution and precipitation of the mineral, the extraframework cations are readily exchangeable (e.g., Newell and Rees, 1983) and water molecules can be reversibly removed from the structure at elevated temperatures (e.g., van Reeuwijk, 1974).

Figure 1-1 depicts the crystal structure of two representative rock-forming zeolites, natrolite and laumontite. The tetrahedral framework sites in zeolites are occupied by Si^{4+} and Al^{3+} (with minor substitution of Fe^{3+}). The extraframework cations balance the net negative charge that exists on the framework due to trivalent Al in the tetrahedral sites. The coordination number and bonding of the extraframework cations vary significantly between different zeolites, among sites in a given zeolite, and between ions (Armbruster and Gunter, 2001). The coordination spheres of these ions are made up of a combination

of framework and water oxygens. The integral presence of water within the crystal structures of zeolites has been known since their discovery (Cronstedt, 1756). Water comprises 8-25% of the mass of zeolites under ambient conditions. In some zeolites like natrolite, there is only one crystallographically distinct water site (Fig. 1-1a); while in some zeolites like laumontite, water is distributed among several crystallographically distinct sites (Fig. 1-1b). Note that water molecules occupy four distinct sites in laumontite, labled W1, W2, W5 and W8 (Artioli and Ståhl, 1993). Sites W2 and W8 are part of the coordination sphere of the Ca^{2+} extraframework ion. Site W5 is hydrogen bonded only to W2 and W8, whereas W1 is hydrogen bonded to both framework oxygens and waters on W2 and W8 (Armbruster and Kohler, 1992). Sequential loss of water molecules from distinct sites appears to be a common phenomenon in zeolites (e.g., Armbruster, 1993; Cruciani et al., 2003). Loss of water can lead to pronounced changes in the structures of the zeolite framework and the positions of extraframework cations. Most zeolites also exhibit contraction and/or collapse of the tetrahedral framework during dehydration.

Zeolites produce abundant water upon heating under atmospheric conditions. A common method of assessing the prograde dehydration of zeolites is by thermogravimetric analysis (TGA), in which mass loss (due to dehydration) of a zeolite sample is monitored as a function of temperature. Some zeolites, like analcime and natrolite, dehydrate continuously with increasing temperature (Fig. 1-2a, corresponding to Fig. 1-1a), yet others like laumontite and heulandite show distinct steps in their dehydration behavior (Fig. 1-2b, corresponding to Fig. 1-1b) (e.g., Alberti and Vezzalini,

1984). These differing behaviors reflect the structural and energetic properties of water molecules within the structures.

Occurrence of Zeolites

Zeolites occur in a wide variety of environments, including two major types of occurrences: 1) macroscopic and microscopic crystals, often in veins, fractures, and vugs within plutonic and volcanic rocks and their metamorphosed equivalents; 2) submicroscopic crystals, commonly distributed in vitroclastic sediments which have undergone diagenetic or low-grade metamorphic processes (Passaglia and Sheppard, 2001). Zeolites can also occur during reactions of aqueous fluids with marine sediments (e.g., Boles and Coombs, 1977), saline lake sediments (e.g., Hay and Moiola, 1963), volcanic tuffs (e.g., Hay and Sheppard, 2001) and soils (e.g., Baldar and Whittig, 1968). Hydrothermal systems often produce zeolites as well with complex parageneses caused by overprinting of diagenetic and metamorphic occurrences (Gottardi, 1989; Neuhoff et al., 1997). Zeolite stability is a sensitive function of pressure, temperature and fluid composition, making them useful indicators of the physical and chemical conditions associated with petroleum resources (e.g., Iijima, 2001), geothermal resources (e.g., Kristmannsdóttir and Tómasson, 1978) and basalt-hosted ore deposits (e.g., Stoiber and Davidson, 1959) in earth's crust. Zeolites and associated authigenic clay minerals can significantly reduce the porosity and permeability of hydrocarbon reservoir rocks, and their presence is often regarded as an economic basement of exploration for oil and gas (e.g., McCulloh et al., 1973; McCulloh and Stewart, 1979). In addition, they are frequently considered as passive barriers in radioactive waste repositories both as sorptive barriers to radionuclide migration and consumption of thermal energy (e.g., Carey and Bish, 1996; Bish et al., 2003).

Industry Application of Zeolites

The high cation-exchange capacities and molecular sieve capabilities make zeolites widely applied in industry, e.g., water softening, catalysis and wastewater treatment (Mumpton, 1977). The relatively large energy storage density of zeolites makes them employed in energy storage and heat pump technologies, where their use instead of activated alumina or silica gel can result in significant reduction of storage weight (e.g., Shigeishi et al., 1979; Scarmozzino et al., 1980; Gopal et al., 1982; Selvidge and Miaoulis, 1990). In agriculture, natural zeolites have been used as soil conditioners, carriers for insecticides and herbicides, remediation agents in contaminated soils, slow-release fertilizers, and dietary supplements in animal nutrition because of their capability of cation exchange, adsorption and their abundance in near surface, sedimentary deposits (Ming, 1985, 1987, 1988; Ming and Mumpton, 1989; Boettinger and Graham, 1995). The unique cation-exchange capabilities of zeolites can be used to remove dissolved cations that affect human and animal health (e.g., NH_4^+) from water by exchanging with biologically acceptable cations such as Na^+, K^+, Mg^{2+}, Ca^{2+} or H^+ (Neveu et al., 1985; Xu, 1990; Pabalan and Bertetti, 1999). The surface area of a zeolite-rich rock is ~10 m^2/g, much bigger than that of quartz sand (~0.01 m^2/g), thus the filtration efficiency of a sand bed can be increased by mixing porous zeolitic rock with it (Grigorieva et al., 1988; Galindo et al., 2000). Zeolites are being used in more and more new technologies, and these potential applications provide numerous possibilities to improve the environment.

Thermodynamics of Dehydration in Zeolites

The response of zeolites to changes in temperature and water vapor pressure is a very important aspect of their behavior and structural changes. Detailed studies of the structural effects accompanying dehydration processes allow evaluation of the changes in

environmental conditions that ultimately lead to structural modification or breakdown (Bish and Carey, 2001). Alberti and Vezzalini (1984) divided zeolites into three categories according to their thermal stabilities. Those with: 1) reversible dehydration accompanied by rearrangement of the extraframework cations and residual water molecules (e.g., chabazite, analcime and mordenite); 2) complete or nearly complete reversible dehydration accompanied by a large distortion of the framework and significant decrease in unit-cell volume (e.g., natrolite, mesolite and laumontite); and 3) irreversible dehydration accompanied by irreversible changes in the framework (e.g., heulandite, barrerite and stilbite).

Equilibrium between a zeolite and water vapor can be represented by a reaction of the form

$$Z{\cdot}nH_2O = Z + n\ H_2O_{vapor} \qquad (1\text{-}1)$$

where $Z{\cdot}nH_2O$ and Z are homologous hydrated (water sites occupied) and dehydrated (water sites vacant) components of a zeolite and *n* is the number of moles of H_2O in the fully hydrated zeolite. Evaluation of the hydration state of zeolites as a function of temperature and pressure requires knowledge of the thermodynamic properties, such as Gibbs energy of reaction ($\Delta G_{r,T,P}$), enthalpy of reaction ($\Delta H_{r,T,P}$) and entropy of reaction ($\Delta S_{r,T,P}$), as well as the relationship between activity and composition. Four basic approaches have been applied in order to determine the thermodynamic properties of zeolite dehydration reactions (cf. Bish and Carey, 2001). The first method involves explicit calculation of $\Delta G_{r,T,P}$ from the known properties of substances in the reaction. For instance, volume of reaction (ΔV_r) can be directly calculated if the molar volumes of $Z{\bullet}nH_2O$ and Z have been determined. This method has been applied to calculation of ΔS_r

and heat capacity of reaction ($\Delta C_{p,r}$) as well from the results of heat capacity (C_p) measurements for homologous hydrates and dehydrated zeolites (Carey, 1993; Ransom and Helgeson, 1994; Neuhoff et al., 2000). In addition, ΔH_r can be determined from the heats of formation of homologous hydrated and dehydrated zeolites determined via thermochemical cycles from heat of solution data (e.g., Johnson et al., 1982, 1983; Ogorodova et al., 1996). The second approach is transposed temperature drop calorimetry (e.g., Navrotsky et al., 1994; Kiseleva et al., 1996, 1997; Shim et al., 1999) in which ΔH_r is determined via a thermochemical cycle involving dehydration of the zeolite at high temperatures (usually ~973 K) and the heat contents of the hydrated and dehydrated zeolites and water. The third method, immersion calorimetry, involves direct calorimetric measurement of ΔH_r as the dehydrated zeolite is immersed in water or humid gas (e.g., Barrer and Cram, 1971; Coughlan and Carroll, 1976; Carey and Bish, 1997; Muller et al., 1998; Petrova et al., 2001). The last method involves fitting equilibrium observations of the water content of a zeolite as a function of temperature and water fugacity, usually determined thermogravimetrically (e.g., Carey and Bish, 1996; Fridriksson et al., 2003) or by pressure titration techniques (Wilkin and Barnes, 1999). Non-linear regression of phase equilibrium observations to the thermodynamic relations can determine the thermodynamic properties at standard conditions ($\Delta G^o_{r,Tref,Pref,}$ $\Delta H^o_{r,Tref,Pref}$, and $\Delta S^o_{r,Tref,Pref}$), but generally requires prior knowledge of $\Delta C_{p,r}$ in order to reduce the number of unknown variables (Carey and Bish, 1996).

Heat Capacities of Hydrous Zeolites

Determination of the temperature dependence of C_p of hydrous minerals at superambient conditions, particularly those that dehydrate continuously with temperature such as zeolites, presents considerable experimental obstacles. Calorimetric

measurements of C_p by adiabatic, drop, or differential scanning calorimetry (DSC) on these materials will inevitably include contributions not only from C_p but also the heat of dehydration. Consequently, there is a paucity of reliable data for C_p of hydrate minerals, which presents considerable complications for assessing the magnitudes of the C_p.

There are two basic approaches that have been taken to address this issue: 1) adjust C_p measured by drop calorimetry for the heat of dehydration determined separately (e.g., Johnson et al., 1982, 1983); and 2) assume that $\Delta C_{p,r}$ is independent of temperature (Barrer, 1978; Carey, 1993), allowing $\Delta C_{p,r}$ to be estimated from C_p for the hydrous and anhydrous phase determined at relatively low temperatures where the dehydration is not an issue. The first approach ignores potential exothermic effects in the calorimetric measurements as the zeolite rehydrates during the drop, potentially leading to overestimation of C_p for hydrous phases (Carey, 1993). The second approach is based on statistical-mechanical arguments that sorption of H_2O into a zeolite should lead to an increase in C_p for this component over that in the vapor phase as a consequence of the loss of translational and rotational degrees of freedom to vibrational modes within the zeolite structure (Barrer, 1978). While this is certainly true, and borne out by some experimental data for $\Delta C_{p,r}$ for complete dehydration of some hydrates (Carey, 1993), there is a paucity of experimental data necessary to test this model. In this study, we measured the temperature dependent heat by isothermal immersion experiments and observed some contradictions with the statistical-mechanical model including second-order phase transition (Johnson et al., 1982; Neuhoff and Bird, 2001) and excess heat capacity (Basler and Lechert, 1972).

Calorimetric Technique

All the calorimetric measurements were performed on the Netzsch STA 449C Jupiter simultaneous thermal analysis system at the University of Florida. A schematic depiction of this system is shown in Fig. 1-3. The core component is a vacuum-tight, liquid nitrogen cooled furnace enclosing a sample carrier housing an electrode for measurement of temperature differences between the sample and a reference pan, generating a heat flux DSC signal and which is connected to a microbalance for thermogravimetric analysis. With respect to the present study, an essential aspect of this setup is that the DSC and TGA signals are recorded simultaneously, which allows the DSC signal to be interpreted directly in terms of water loss or gain to the sample as measured by TGA. The temperature range for the furnace is 120 to 1050 K; temperature can be maintained within this range to a precision of better than 1 K and for dynamic analysis can be run at controlled heating or cooling rates of up to 50 K/minute. Samples as large as 5 g and as small as 1 mg can be investigated, although sample sizes of the order of a few 10's of mg are optimal. Mass changes as small as 0.1 μg can be detected. Calorimetric precision varies with experimental conditions and the amount of heat involved; instrument specifications call for C_p precision on the order of 2.5% and heat of reaction precision on the order of 3%. Precision obtained for the experiments proposed in our study is described further below. Temperature and caloric calibration is performed by measuring the melting temperatures and heats of fusion of high purity metal standards and C_p of sapphire disks (cf. Höhne et al., 1990; Sarge et al., 1994; Sabbah et al., 1999). Temperature, DSC, and TGA signals are sent via cable to a personal computer for recording and data analysis.

Experimental conditions can be controlled with respect to not only temperature but also pressure. Experiments can be run under closed system conditions at total pressures ranging from atmospheric to vacuums of 10^{-4} Torr, although typical operation involves a flowing gas atmosphere at atmospheric pressure. Gas composition and flow rate are controlled externally via mass flow controllers. Gases used in the experiments are ultra-high purity He (for subambient temperatures) and N_2 (for C_p measurements and measurements under controlled humidity conditions). Humidity is generated by bubbling N_2 through distilled water at a constant temperature, with water vapor pressure (P_{H2O}) varied by mixing H_2O-saturated and dry N_2 gas in different proportions. Humidity on the outflow end of the furnace is constantly monitored and recorded by a Sable Systems RH-100 flow-through dewpoint/relative humidity analyzer (1% accuracy in P_{H2O} down to 1 Pa).

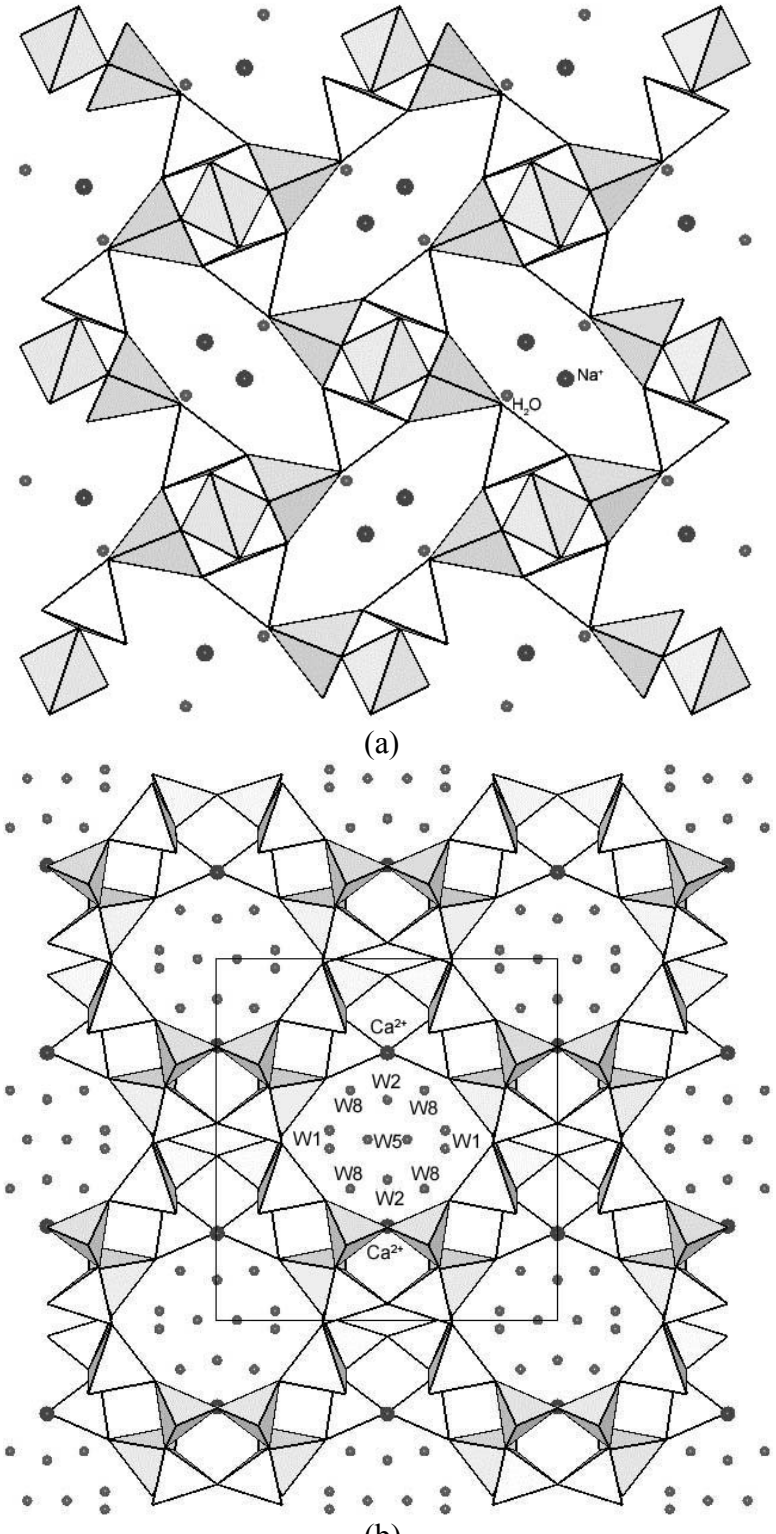

(a)

(b)

Figure 1-1. View of the crystal structures of natrolite (a) (after Peacor, 1973) and laumontite (b) (after Fridriksson et al., 2003) projected along the *c* axis. Natrolite has only one water site, whereas laumontite has four water sites: W1, W2, W5 and W8.

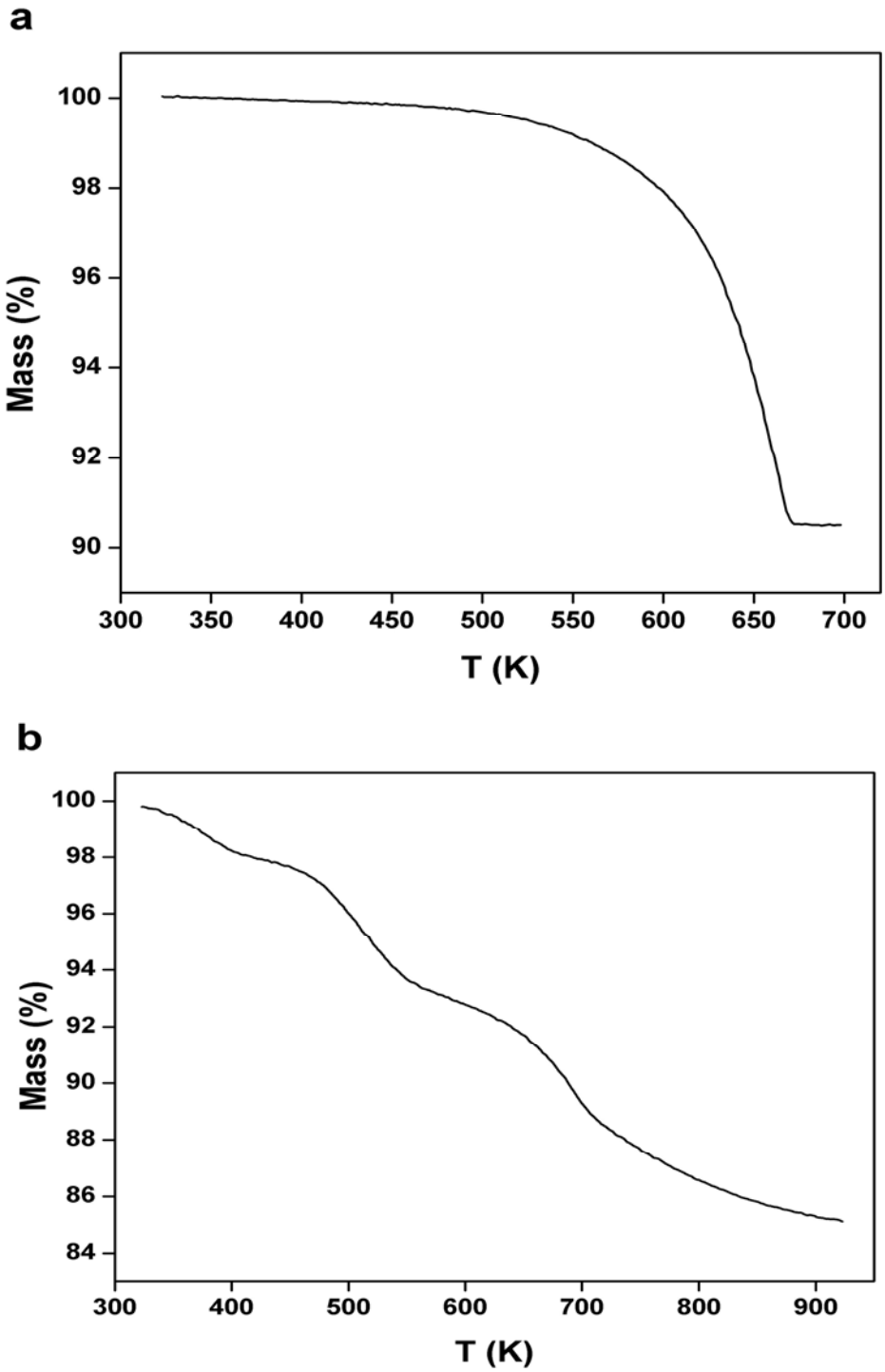

Figure 1-2. Thermogravimetric analysis (TGA) curves depicting the change in mass with increasing temperature of natrolite (a) and laumontite (b). Natrolite contains a single water site and exhibits one continuous dehydration curve, whereas laumontite has several water sites that dehydrate under different conditions as reflected in the inflections observed in the mass loss as a function of temperature.

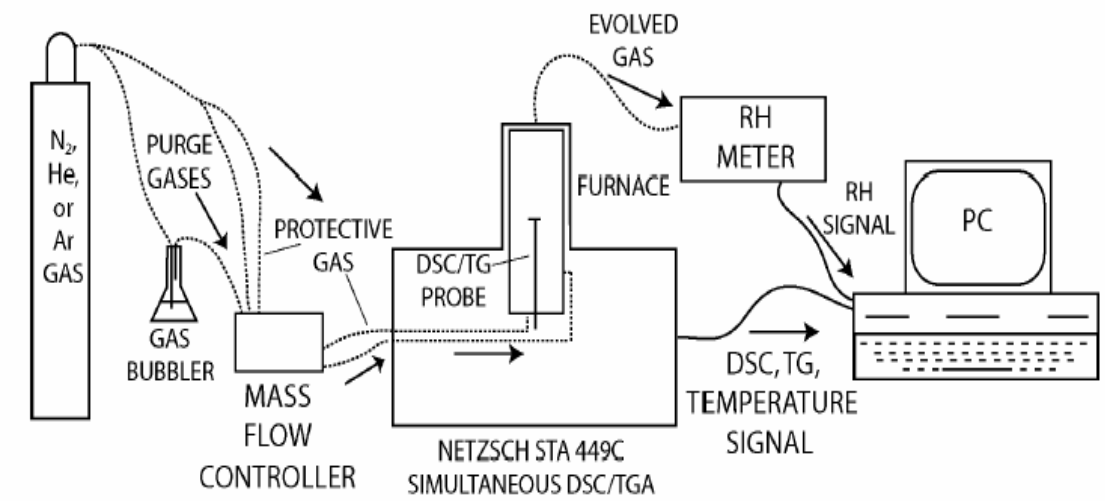

Figure 1-3. Schematic representation of the simultaneous DSC/TGA system. Dashed curves represent gas lines; solid curves represent data transfer cables between the instruments and the computer.

CHAPTER 2
ENTHALPY OF HYDRATION IN ANALCIME

Introduction

Analcime, nominally $NaAlSi_2O_6 \cdot H_2O$, is one of the most common rock-forming zeolites. It appears to be stable over a considerable range of temperature and pressure conditions, thus it occurs in a very wide range of geologic settings. Analcime generally forms during low grade metamorphism of plutonic and volcanic rocks, as a product of reaction between saline solutions and sediments in alkaline lakes (e.g., Hay and Moiola, 1963; Hay, 1966; Coombs and Whetten, 1967; Iijima and Harada, 1968; Surdam and Sheppard, 1978), and as phenocrysts in alkalic igneous rocks (e.g., Wilkinson and Hensel, 1994). Although recent progress has been made in assessing the stability of analcime in low-temeprature environments (e.g., Neuhoff et al., 2004), phase equilibria observations at elevated temperature and pressure are often inconsistent with each other (cf. Thompson, 1973). In large part, this appears to be due to complications arising from solid solution in analcime, particularly with respect to its variable water content due to progressive dehydration with increasing temperature (e.g., Helgeson et al., 1978)

Dehydration of analcime is a relatively simple one step process because water molecules occupy only one crystallographically distinct site (Fig. 1-1, Mazzi and Galli, 1978). Several authors have studied the hydration-dehydration thermodynamics of analcime (e.g., King, 1955; King and Weller, 1961; Robie et al., 1979; Helgeson et al., 1978; Johnson et al., 1982; Ogorodova et al., 1996; Bish and Carey, 2001). Application of these data to predicting the hydration state of analcime is complicated by a lack of

understanding of the temperature dependence of these properties, which largely relies on assessing of the change in heat capacity brought about by dehydration. Experimental determinations of the heat capacities (C_p) of the hydrated and dehydrated forms of these minerals (e.g., King, 1955; King and Weller, 1961; Pankratz, 1968; Johnson et al., 1982) are complicated because the calorimetric measurements at superambient temperatures generally include contributions not only from C_p but also the heat of dehydration. In the absence of reliable data, an assumption that C_p of dehydration in analcime is independent of temperature (Barrer, 1978; Carey, 1993) was made based on the statistical-mechanical arguments that much of the difference in C_p between absorbed water and the gas phase is caused by the loss of some translational and rotational degrees of freedom to weak vibrational modes within the zeolite structure. Although the C_p results of some stable zeolites near room temperature are consistent with this assumption (Carey, 1993), no other approaches have been used to test it.

In the present investigation, the isothermal heats of hydration in analcime were measured over a range of temperature under constant water vapor pressure, and a general behavior of the heat capacity of hydration ($\Delta C_{p,r}$) for analcime dehydration was obtained. In addition, the heat capacities of hydrated and dehydrated analcime were determined as a function of temperature by differential scanning calorimetry (DSC), and the results were used to calculate $\Delta C_{p,r}$ based on the statistical-mechanical model. Comparison of these two methods is used to evaluate the appropriateness of the assumption that $\Delta C_{p,r}$ is not a function of temperature.

Methods

Sample and Characterization

The sample of analcime was collected from a zeolite-facies metabasalt outcrop at Maniilat on the island of Qeqertarsuaq in West Greenland (Neuhoff et al., 2003), and prepared from a 1.5 cm euhedral crystal of opaque analcime. Separates of analcime were hand picked, ground in an agate mortar, and sieved to a 20-40 μm size fraction. Phase identity and purity were confirmed by X-ray powder diffraction. A split of this sample was previously used and characterized in the ^{29}Si magic angle spinning nuclear magnetic resonance (MAS NMR) study of Neuhoff et al. (2003; Sample ANA002). Electron probe microanalysis indicated a composition of $(NaAl)_{0.95}Si_{2.05}O_6 \cdot 1.024H_2O$, although the ^{29}Si MAS NMR results indicate a slightly less Si-rich composition of $(NaAl)_{0.97}Si_{2.03}O_6 \cdot 1.015H_2O$. The latter value was chosen as more representative of the bulk composition (cf. Neuhoff et al., 2004) and consistent with the water content. Water content of the sample was determined by thermogravimetric heating to 1023 K after the equilibration with a room temperature atmosphere of 50% relative humidity (RH), and the mass loss was measured to be 8.29% of the total sample. This value is close to water content calculated from the compositions determined by ^{29}Si MAS NMR, 8.32% (cf. Neuhoff et al., 2004).

Absorption Calorimetry

Heats of hydration as a function of temperature were determined using an isothermal DSC-based immersion technique on the Netzsch STA 449C Jupiter simultaneous DSC-thermogravimetric analysis (TGA) system at the University of Florida as described by Neuhoff and Wang (2006). This approach combines the benefits of DSC and gas absorption calorimetry. Twenty to 30 mg of hydrated analcime were placed into a

Pt-Rh crucible for each run. The sample was dehydrated by scanning heating from 298 to 873 K at the rate of 15 K/min and then allowed to cool to the experimental temperature. A purge of dry N_2 was maintained at a flow rate of 50 ml/min during this period. After equilibration (20-40 min.) at this temperature under dry N_2 until both DSC and TGA baselines stabilized, the gas stream was changed to humid N_2 which was generated by bubbling ultrapure N_2 gas through a saturated NaCl solution. In order to reduce the change of DSC baseline, the flow rate of humid N_2 was maintained at 30 ml/min and the corresponding water vapor pressure in the furnace was ~12 mbar. Under this condition the sample was allowed to react until the DSC trace became relatively flat. Repeated experiments on one analcime sample gave virtually identical results, indicating that the sorption capacity of analcime was not affected by dehydration and hydration. Consequently, some of the data at different temperatures were measured from the same sample aliquot. During the experiment, the sample of dehydrated analcime could only reabsorb less than 5% of its mass, as opposed to ~9.1% mass gain for complete rehydration. Therefore, under current water vapor pressure we can only directly measure partial molar enthalpies of hydration (Δh_{hyd}) for analcime.

Heat Capacity Measurements

The heat capacities of hydrated and dehydrated analcime were also determined by DSC also on the simultaneous DSC-TGA system. Each experiment consisted of four separate runs: 1) determination of background and baseline by measurement of an empty crucible; 2) DSC measurement of a standard (sapphire); 3) scanning heating of hydrated analcime and 4) scanning heating of dehydrated analcime. A sample of approximately 27 mg was packed into a covered Pt-Rh crucible before step 3 and kept to the end of the experiment. Data were collected in the range of 298 to 873 K at a scanning rate of 15

K/min. A purge of dry N_2 was used during the experiment to keep the relative humidity below 1%, and the gas flow was maintained at ~30 ml/min using mass flow controllers. The furnace was heated to 873 K in each run and then cooled back to room temperature by liquid N_2 before the next step. During heating, hydrated analcime lost mass with increasing temperature and finally became completely dehydrated. The resulting dehydrated analcime was kept in an environment of dry N_2 to avoid rehydration during cooling to room temperature and then measured by scanning heating again. Heat capacity of the sample as a function of temperature was calculated by

$$C_p = \frac{m_{std}}{m_s} \times \frac{DSC_s - DSC_b}{DSC_{std} - DSC_b} \times C_{p,\,std} \qquad (2\text{-}1)$$

where m_s is the mass of sample, m_{std} is the mass of standard (27.314 mg), DSC_s, DSC_{std} and DSC_b are for sample, standard and baseline respectively. Triplicate calorimetric measurements were conducted and averaged. Based on previous measurements in this lab the precision was taken to be 1% of C_p.

Results

Enthalpy of Hydration in Analcime

An example of TGA and DSC response of analcime during immersion in water vapor at 403 K is shown in Fig. 2-2. It is observed that the hydration of analcime is initially relatively rapid (as shown by the peak in the first derivative of the TGA signal, dTGA) and then decays exponentially. After about 120 min. the reaction slowed to a point where the DSC signal had decayed to near baseline level and essentially invariant with respect to time even though sample could keep on absorbing H_2O if the experiment continued. The slow rate of the reaction is also reflected in the near-zero value of dTGA.

It can be seen in Fig. 2-2 that the DSC and dTGA data are strongly correlated. These data are plotted against each other in Fig. 2-3, and the slope of the linear regression is proportional to Δh_{hyd}. Consequently, the partial molar enthalpies of hydration can be calculated by the equation

$$\Delta h_{hyd} = k\,(\mathrm{dDSC/dm})\,(MW_{H_2O}) \qquad (2\text{-}2)$$

where k is the caloric calibration factor (in mW/μV), dDSC/dm is the slope in Fig. 2-3, and MW_{H_2O} is the molecular weight of water. The y-intercept of the regression represents the DSC signal when dTGA = 0; i.e., the baseline at the end of reaction. The partial molar enthalpy of hydration in analcime calculated by this method has relatively large error because of the oscillation of DSC and dTGA signals. Using the position of the baseline derived by linear regression of the DSC and TGA signal provides another approach to determine the Δh_{hyd}. Cumulative, baseline-corrected DSC response plotted against cumulative mass of absorbed H_2O also leads to a linear dependence, the slope of which is also equivalent to Δh_{hyd} (Fig. 2-4).

The results of partial molar enthalpy at ten different temperatures calculated by both methods are listed in Table 2-1. Most of the values of Δh_{hyd1} and Δh_{hyd2} at the same temperature are close to each other (within 1.5% difference), illustrating the general repeatability of this method. For some temperatures the difference between Δh_{hyd1} and Δh_{hyd2} is relatively big; this may result from the uncertainty of the baseline caused by the oscillation of the signals. The temperature dependence of Δh_{hyd} are illustrated in Fig. 2-5. The errors include the part from standard deviation of the values and that from the calorimetric calibration (1% of the results). It can be seen that within the analysis error

the Δh_{hyd} at different temperatures have little change except the one at 528 K, which may indicate a trend of abrupt decrease and increase of Δh_{hyd} with increasing temperature.

Heat Capacities of Hydrated and Dehydrated Analcime

Figure 2-6 shows TGA and DSC traces of hydrated and dehydrated analcime obtained during scanning heating. Dehydration of analcime is accompanied by a mass loss from ~350 K to 743 K, which is also indicated by the positive inflection of the DSC curve. The TGA curve is continuous and suggests only one stage of dehydration, consistent with previous observations that only one energetically distinct water site is presented in analcime (e.g., van Reeuwijk, 1974; Bish and Carey, 2001) and the crystal chemical considerations listed above. Unlike the TGA trace for hydrated analcime, there is no mass change for dehydrated analcime during scanning heating, showing that the sample has been completely dehydrated in the first run.

Calculated C_p for hydrated and dehydrated analcime are compared in Fig. 2-7. The heat capacity of hydrated analcime is relatively insensitive to the temperature below ~399 K, but increases quickly after that because of the contribution of dehydration. For dehydrated analcime the heat measurement only includes the contribution from C_p, so the trace of C_p increases very slowly with increasing temperature, and in a nearly linear fashion.

Discussion

Comparison of Present Results with Previous Studies

Low-temperature (below 350 K) C_p measurements on analcime have been reported previously (King, 1955; King and Weller, 1961; Johnson et al., 1982). The data of low-temperature C_p were directly measured by adiabatic calorimetry. In addition, Johnson et al. (1982) also assessed the C_p for analcime above 350 K by drop calorimetry. The

present results of C_p of hydrated analcime below 350 K are in good agreement with those from Johnson et al. (1982). For instance, at 298 K the difference between the two values is only ~0.6%. However, above 350 K, C_p measured in the present study is higher than those of Johnson et al. (1982) because of the strong dehydration effect on the DSC signal. As for the C_p of dehydrated analcime, the present results are closer to those from Johnson et al. (1982) at low temperatures than at high temperatures, but are generally. Examination of the method that Johnson et al. (1982) used to determine the C_p of dehydrated analcime suggests that the cause is that their sample was not completely anhydrous.

The enthalpy of hydration in analcime at 298 K has been determined by several authors using different methods (Johnson et al., 1982; Ogorodova et al., 1996; Barany, 1962; Bish and Carey, 2001), and the results are listed in Table 2-3. Especially, Ogorodova et al. (1996) found that enthalpy of formation of analcime is linearly dependent on the degree of hydration in analcime, indicating that there are no excess contributions to the enthalpy across the solid solution between hydrated and dehydrated analcime. Therefore, it is reasonable to assume that the integral molar enthalpy of hydration (ΔH_{hyd}) should equal Δh_{hyd} at the same temperature. In general, present values of ΔH_{hyd} within error increase with increasing temperature below 463 K and the difference between the values of 403 K and 463 K is relatively small (Table 2-1, Fig. 2-5). The result of ΔH_{hyd} at 298 K interpreted from present data is in good agreement with previous studies.

Temperature Dependence of Heat of Hydration

The enthalpies of hydration in analcime shown in Fig. 2-5 as a function of temperature can be divided into two regions. At temperatures below ~470 K, Δh_{hyd} is

relatively insensitive to the temperature. In this range of temperature Δh_{hyd} generally increases with increasing temperature. At temperatures above ~470 K, the abnormal value of Δh_{hyd} at 528 K may indicate that a dramatic change occurs to Δh_{hyd}. It decreases abruptly at ~470 K and continues to drop rapidly with increasing temperature. At even higher temperatures Δh_{hyd} starts to increase again with increasing temperature. The temperature dependence of Δh_{hyd} can be used to assess the magnitude of $\Delta C_{p,r}$ via the relationship

$$\Delta C_{p,r} = \left(\frac{\partial h_{hyd}}{\partial T}\right)_p \tag{2-3}$$

The measurement of C_p for hydrated analcime in this study is greatly affected by the contribution from dehydration above ~350 K, whereas this effect is smaller in the drop calorimetric method according to the data of Johnson et al (1982). As for the dehydrated analcime, our samples were run under a completely dry condition, so our C_p data for dehydrated analcime is reliable. Considering the similar compositions of the analcime samples used in the experiments of Johnson et al. (1982) and this study, we combine the C_p data of hydrated analcime from Johnson et al. (1982) and our data of dehydrated analcime to estimate the $\Delta C_{p,r}$ for analcime hydration.

Equilibrium between dehydrated and hydrated analcime can be represented by a hydration of the form

$$(NaAl)_{0.97}Si_{2.03}O_6 + 1.015\ H_2O_{vapor} = (NaAl)_{0.97}Si_{2.03}O_6 \cdot 1.015H_2O \tag{2-4}$$

Thus, heat capacity of hydration can be calculated by the following equation

$$\Delta C_{p,r} = (C_{p,ana} - C_{p,deana} - 1.015C_{p,H2O}) / 1.015 \tag{2-5}$$

where $C_{p,ana}$ and $C_{p,deana}$ are the heat capacities of hydrated and dehydrated analcime, respectively; $C_{p,H2O}$ is the heat capacity of water vapor taken from Robie and Hemingway

(1995). The results of $\Delta C_{p,r}$ derived from our data and the combined data are both plotted in Fig. 2-8 as a function of temperature. Note that both curves have a relatively flat part in the relatively low temperature range (e.g., 298-350 K for results of our data and 351-430 K for results of combined data), in which dehydration effect is much smaller than that above 430 K to the C_p measurement. In this region, $\Delta C_{p,r}$ is insensitive to temperature and the two results have similar magnitudes, 12-15 J/molK (about 1.5R-2R, R is the gas constant, equals 8.314 J/molK). This is quite similar to the value obtained by linear regression of Δh_{hyd} below 470 K, which indiates a value of $\Delta C_{p,r}$ of 17.1 ± 12.4 J/molK (Fig. 2-9).

Above 470 K, the decrease and then increase in Δhhyd with increasing temperature indicates that ΔCp,r becomes negative and then positive again. This is indicative of a phase transition in hydrated analcime. This behavior is not apparent in ΔCp,r calculated from Cp data, as the transition is masked by the effects of dehydration that lead to erroneously large values of Cp for hydrated analcime.

Behavior of Heat Capacity of Hydration

Heat capacities of hydrated zeolites are difficult to measure, especially at relatively high temperatures. In the absence of the reliable data for the hydrations of zeolites, Barrer (1978) discussed a statistical-mechanical model for heat capacity of molecular gases absorbed in zeolites to simplify the calculation of $\Delta C_{p,r}$. This model argues that the sorption of H_2O into a zeolite should lead to an increase in C_p for this component because of the loss of some translational and rotational degrees of freedom to week vibrational modes within the zeolite structure (Carey, 1993). The difference in C_p between absorbed H_2O and gas phase can be determined by the number of vibrational modes gained by the absorbed species. With this model, the heat capacity of the absorbed species increases by

R/2 for each saturated vibrational mode gained, and the heat capacity difference between absorbed and free H_2O is limited between zero and 3R (R is the gas constant, 8.314 J/molK) (Bish and Carey, 2001). Based on the statistical-mechanical model, an assumption can be made that $\Delta C_{p,r}$ of hydration in zeolites is independent of temperature and the value is n*R/2 ($0 \leq n \leq 6$). In the case of analcime, the $\Delta C_{p,r}$ calculated from combined data is almost constant in the low temperature range, for instance, 350-430 K, in which the dehydration effect can be ignored. That means the heat capacity of hydration in analcime is independent of temperature and the magnitude is approximately 1.5R-2R. Thus, it appears that the statistical-mechanical model is valid in this temperature range. The enthalpies of hydration at five different temperatures between 373 and 463 K show an almost linear relationship with temperature, indicating that $\Delta C_{p,r}$ in this region is generally independent of temperature. In addition, the magnitude of $\Delta C_{p,r}$ determined by this approach is approximately 2R, which agrees with that of the calorimetric $\Delta C_{p,r}$ within error.

Enthalpies of hydration measured above 463 K show clear evidence of a phase transition in analcime. Although the limited resolution afforded by the Δh_{hyd} measurements precludes a rigorous assessment of the nature of this transition, the general shape implied by the results in Fig. 2-5 indicates that this transition is probably a λ-type, second order transition. This kind of phase transition has previously been found in wairakite (Neuhoff and Keddy, 2004) at slightly lower temperatures, in which $\Delta C_{p,r}$ becomes negative after the transition (dehydration precludes assessment of the behavior at higher temperatures). It appears that almost identical behavior occurs in analcime. Neither the calorimetric results nor the statistical-mechanical model predict this phase

transition, underscoring the need for measurements such as those conducted in this study. If more data of Δh_{hyd} are available, an empirical equation for $\Delta C_{p,r}$ may be extrapolated by the first derivative of Δh_{hyd}.

Table 2-1. Isothermal immersion calorimetric data for analcime.

T (K)	Sample mass (mg)	Duration[1] (min)	% H_2O uptake[2]	Δh_{hyd1}[3] (kJ/mol)	Δh_{hyd2}[4] (kJ/mol)	$\Delta h_{hyd,ave}$[5] (kJ/mol)	±Error (kJ/mol)
403	22.93	73	1.40	-86.29	-86.45	-85.69	1.02
403	25.67	97	1.60	-85.61	-85.15		
403	29.60	95	1.62	-85.39	-85.27		
417	25.67	82	1.80	-86.07	-85.91		
417	27.46	83	1.94	-85.44	-85.19	-85.12	1.23
417	29.13	110	2.00	-83.93	-84.20		
432	22.93	110	2.40	-85.35	-84.94		
432	25.67	100	2.38	-85.14	-84.80	-84.98	0.88
432	29.13	100	2.59	-84.77	-84.87		
446	22.91	150	3.14	-85.55	-84.77		
446	22.93	69	2.25	-84.70	-83.62	-85.42	1.35
446	29.14	74	2.35	-86.93	-86.46		
446	29.13	115	2.63	-85.71	-85.61		
463	22.93	79	2.76	-84.75	-84.12		
463	29.14	84	2.81	-84.85	-84.47	-85.29	1.20
463	29.13	100	2.83	-86.30	-85.78		
463	29.60	108	3.08	-86.26	-85.81		
470	25.67	110	2.98	-86.51	-85.99	-85.05	1.64
470	27.76	260	3.70	-83.95	-83.75		
490	27.76	120	3.29	-85.93	-86.18		
490	29.14	110	3.03	-87.91	-88.00	-87.35	1.34
490	29.13	67	2.64	-87.87	-88.21		
499	29.14	100	2.92	-87.73	-87.11	-87.42	0.94
499	30.99	110	3.02	-87.7	-87.15		
528	29.13	105	2.68	-89.16	-89.07	-89.17	0.96
528	29.14	110	2.49	-89.64	-88.82		
548	25.02	116	2.05	-88.68	-87.70		
548	29.13	130	2.05	-88.08	-87.24	-87.82	1.03
548	33.06	120	1.97	-87.97	-87.26		

[1]Duration of immersion portion of experiment used in data regresion. [2]Mass of the H_2O (in percentage) absorbed. [3]Partial molar enthalpy of hydration in analcime calculated by DSC and dTGA. [4]Partial molar enthalpy of hydration in analcime calculated from cumulative, baseline-corrected DSC and mass of absorbed H_2O. [5]Average partial molar enthalpy of hydration in analcime, calculated by averaging values of Δh_{hyd1} and Δh_{hyd2} at the same temperature.

Table 2-2. Heat capacities of hydrated and dehydrated analcime, steam, and hydration of analcime at different temperatures.

T (K)	$C_{p,\,an}$[1] (J/molK)	$C_{p,\,an}$[2] (J/molK)	$C_{p,\,dean}$[1] (J/molK)	$C_{p,\,H2O}$[3] (J/molK)	$\Delta C_{p,\,r}$[4] (J/mol-H_2O/K)	$\Delta C_{p,\,r}$[5] (J/mol-H_2O/K)
298	210.44		162.32	33.59	13.81	
300	211.01		162.95	33.59	13.77	
310	213.54		165.92	33.58	13.33	
320	216.74		168.47	33.59	13.97	
330	219.42		171.25	33.61	13.85	
340	222.37		173.70	33.64	14.31	
350	225.43	223.11	175.96	33.69	15.05	12.77
360	228.29	225.25	178.56	33.74	15.25	12.26
370	231.09	227.67	180.98	33.80	15.56	12.20
380	234.20	230.13	183.12	33.88	16.45	12.45
390	237.62	232.63	185.45	33.95	17.45	12.53
400	241.94	235.16	187.77	34.04	19.33	12.64
410	246.84	237.71	190.30	34.13	21.58	12.59
420	252.23	240.30	192.94	34.22	24.19	12.43
430	258.35	242.90	194.82	34.32	28.27	13.05
440	264.89	245.53	196.51	34.42	32.96	13.88
450	272.64	248.18	198.58	34.53	38.44	14.34
460	281.53	250.85	200.60	34.63	45.10	14.88
470	291.85	253.54	202.34	34.75	53.44	15.69
480	304.33	256.24	204.54	34.86	63.46	16.08
490	318.08	258.95	207.08	34.97	74.39	16.13
500	332.91	261.68	208.75	35.09	87.23	17.05
510	350.21	264.42	210.21	35.21	102.72	18.20
520	368.18	267.17	211.76	35.33	118.77	19.26
530	386.85	269.93	213.41	35.46	135.41	20.23
540	880.35	272.70	215.72	35.58	619.22	20.56
550	429.12	275.48	217.98	35.71	172.32	20.95
560	452.40	278.27	220.04	35.83	193.09	21.53
570	478.75	281.06	222.03	35.96	216.97	22.21
580	509.19	283.87	223.13	36.09	245.75	23.75
590	547.49	286.67	225.03	36.21	281.49	24.52
600	594.89	289.49	225.81	36.34	327.29	26.40
610	656.84	292.31	227.57	36.47	386.46	27.31
620	733.15	295.14	228.74	36.60	460.35	28.81
630	811.90	297.97	229.89	36.73	536.68	30.34
640	880.35	300.81	230.09	36.87	603.78	32.80

[1]$C_{p,\,an}$ and $C_{p,\,dean}$ are heat capacities of hydrated and dehydrated analcime collected in this study. [2]Heat capacity of hydrated analcime from Johnson et al (1982). [3]Heat capacity of $H_2O_{(g)}$ from Robie and Hemingway (1995). [4]Heat capacity of hydration in analcime calculated by $C_{p,\,an}$[1] and $C_{p,\,dean}$[1]. [5]Heat capacity of hydration in analcime calculated by $C_{p,\,an}$[2] and $C_{p,\,dean}$[1].

Table 2-3. Enthalpy of hydration in analcime.

Composition	Method[1]	Temperature (K)	ΔH_{hyd} (kJ/mol)
$(NaAl)_{0.96}Si_{2.04}O_6 \cdot H_2O$	HF	298.15	-84.9 ± 4.0[2]
$(NaAl)_{0.95}Si_{2.05}O_6 \cdot H_2O$	TTD	298.15	-85.7 ± 1.9[3]
$(NaAl)_{0.96}Si_{2.04}O_6 \cdot H_2O$	HF	298.15	-73.9 ± 4.4[4]
$NaAlSi_2O_6 \cdot H_2O$	PE	298.15	-80.4[5]
Not reported	PE	569.15	-83.7 ± 4.0[6]
Not reported	PE	660.15	-86.6 ± 4.0[6]

[1]Methods: HF: determination of enthalpies of formation of hydrated and dehydrated homologs by HF solution calorimetry; TTD: transposed temperature drop calorimetry; PE: retrieval from phase equilibrium observations.
[2]Johnson *et al.* (1982)
[3]Ogorodova *et al.* (1996)
[4]Calculated from data of Barany (1962) as recalculated by Johnson *et al.* (1982)
[5]Retrieved by Bish and Carey (2001) from observations of Balgord and Roy (1973)
[6]van Reeuwijk (1974)

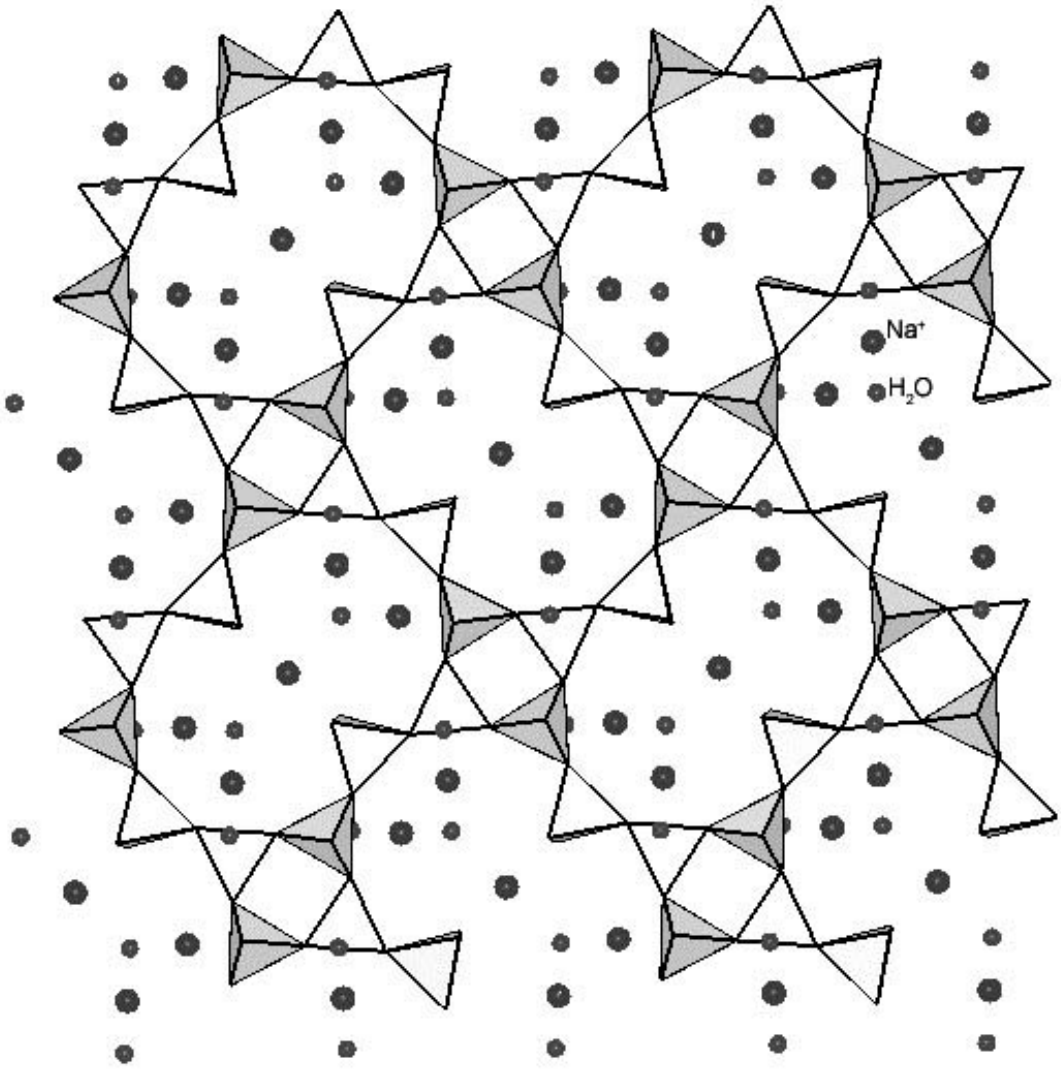

Figure 2-1. Crystal structure of analcime viewed down the *b* crystallographic axis (after Mazzi and Galli, 1978). The framework of Si- and Al- centered tetrahedra are surrounded by four oxygens. The big spheres denote the positions of Na^+ ions. The small spheres are the positions of water molecules.

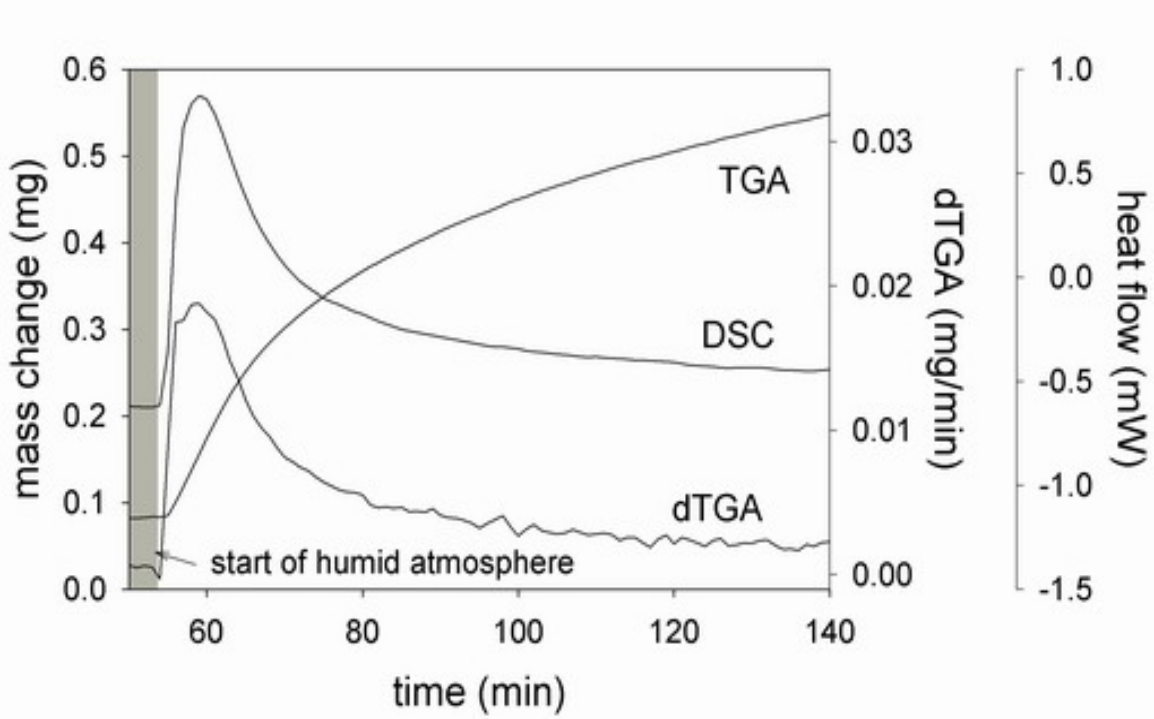

Figure 2-2. Example isothermal immersion experiment on analcime at 403K. Simultaneously-recorded TGA and DSC signals for analcime as a function of temperature. The first derivative of the TG curve is given by the curve labeled dTGA. Region of the gray box denotes initial equilibration of sample at experimental temperature under dry N_2. The rest of the experiment was conducted in the presence of a flow of humidified N_2.

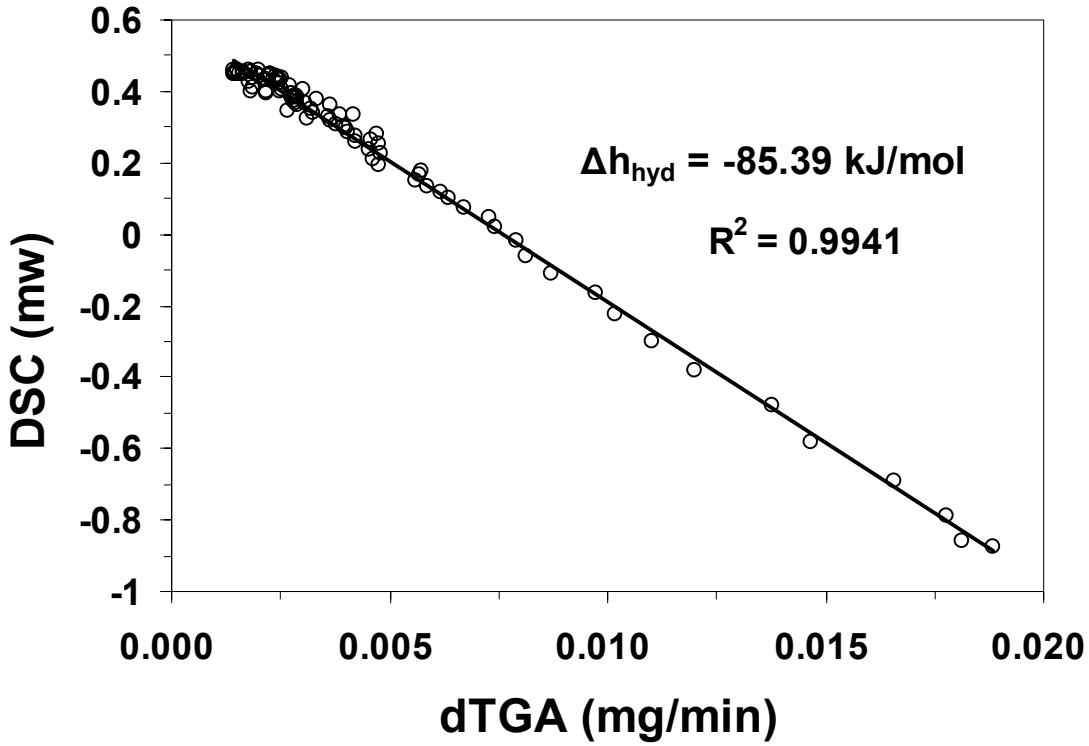

Figure 2-3. Plot of DSC versus dTGA for the experimental results shown in Fig. 2-2. The slope of the linear regression shown in the figure is proportional to Δh_{hyd}.

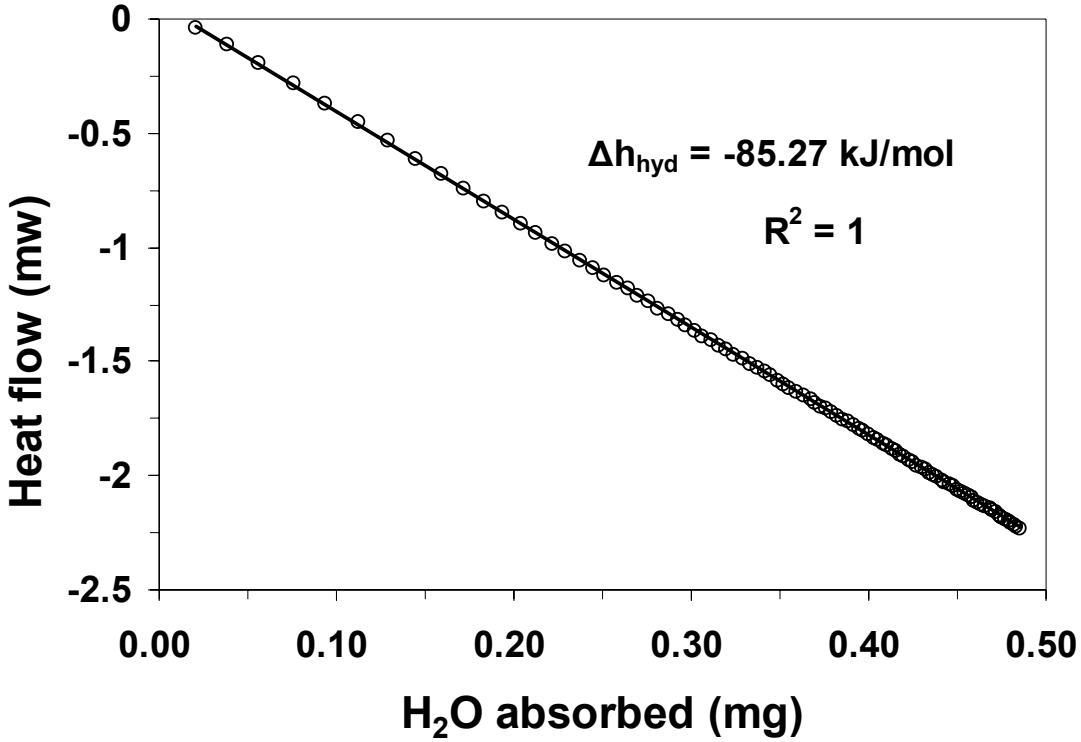

Figure 2-4. Heat evolved during absorption of water into analcime as a function of mass absorbed. The slope of the linear equation can be transformed to Δh_{hyd}.

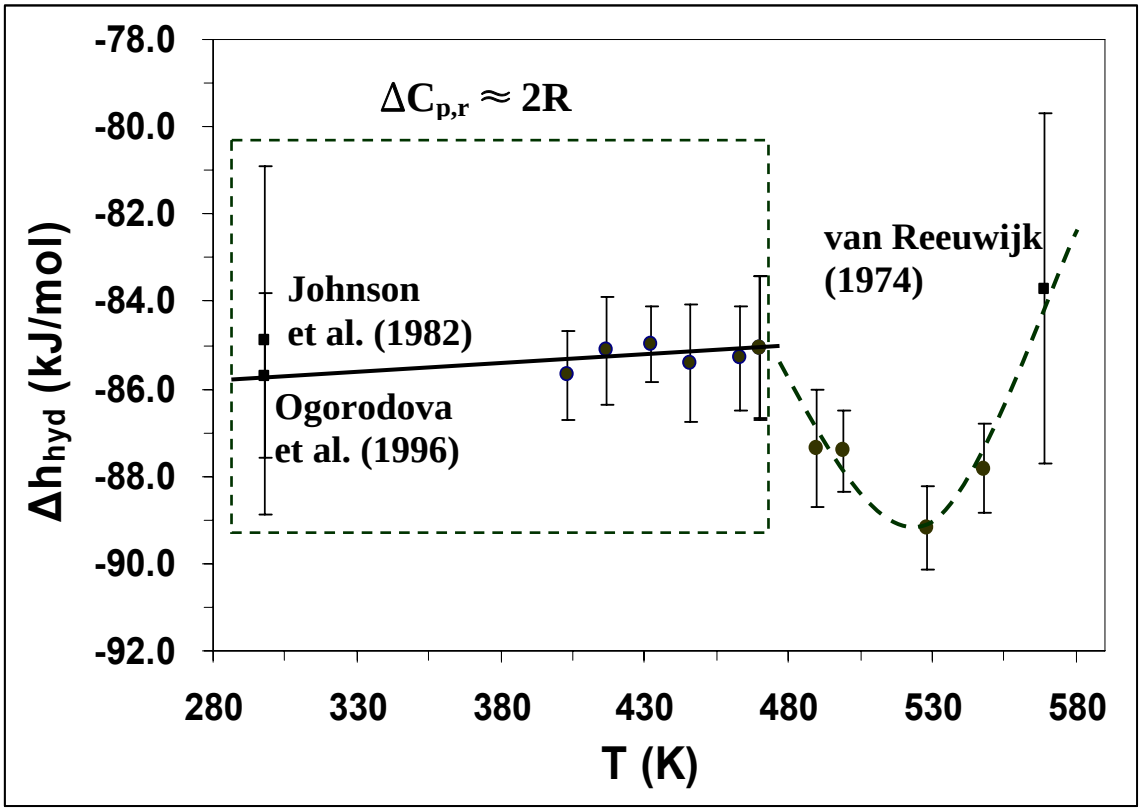

Figure 2-5. Enthalpy of hydration in analcime as a function of temperature. The value of Δh_{hyd} at 528 K is abnormal, may imply a trend that Δh_{hyd} decreases and then increases rapidly with increasing temperature, indicating a phase transition.

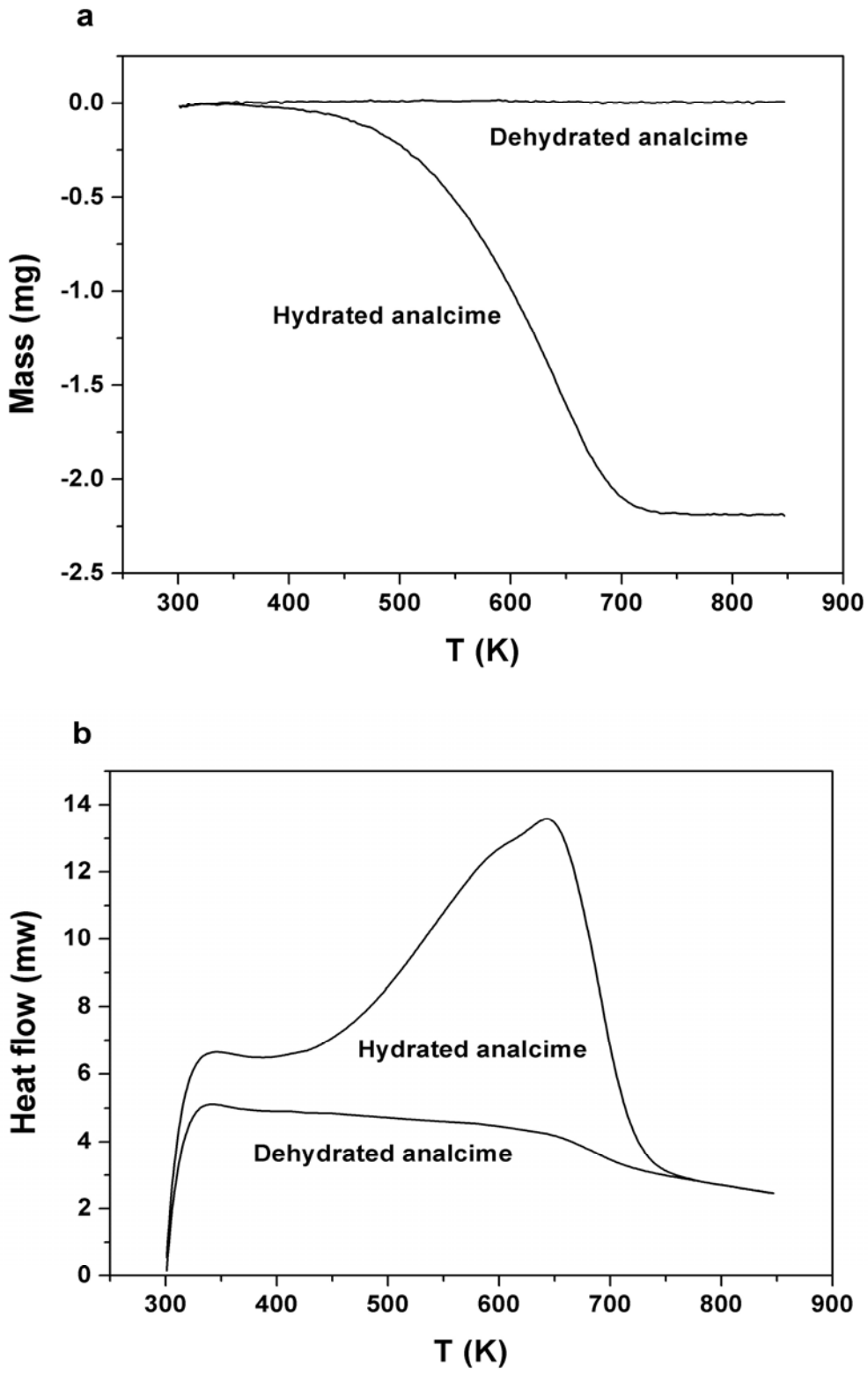

Figure 2-6. The mass change (a) and DSC response (b) of hydrated and dehydrated analcime collected at a scanning rate of 15 K/min under ultrapure N_2.

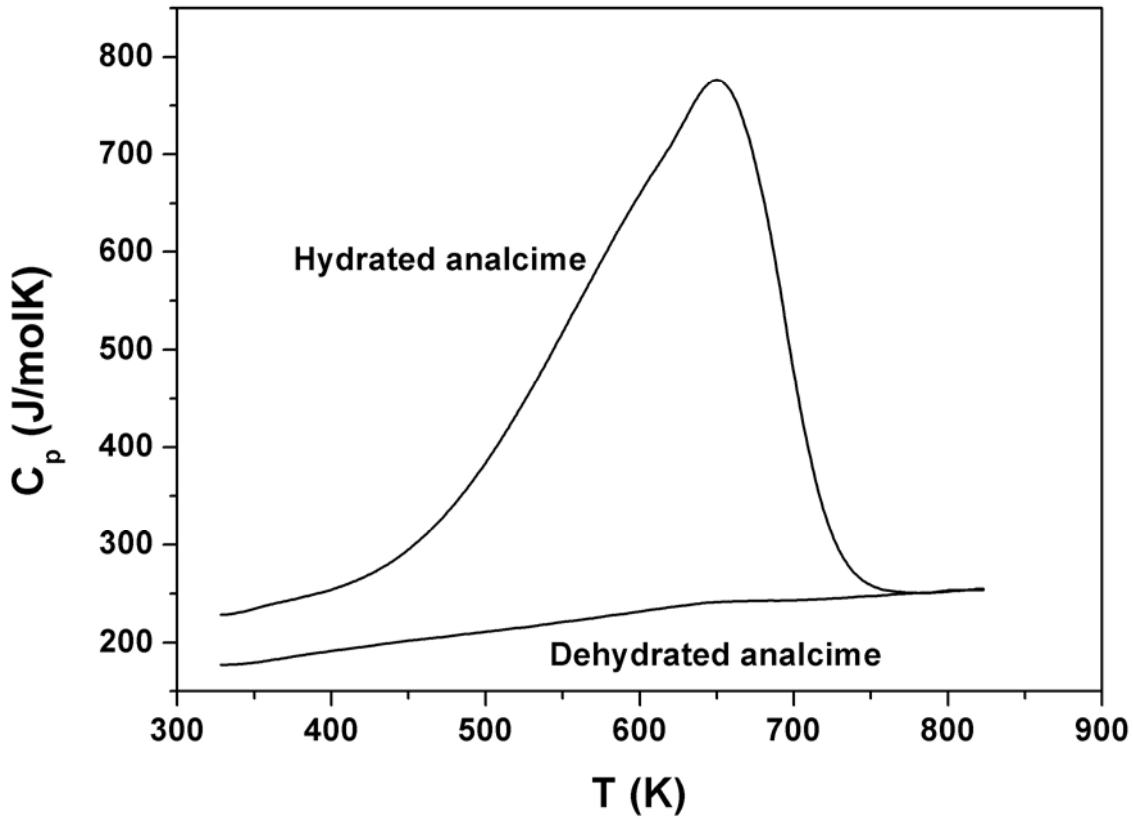

Figure 2-7. Experimental C_p data as a function of temperature for hydrated and dehydrated analcime.

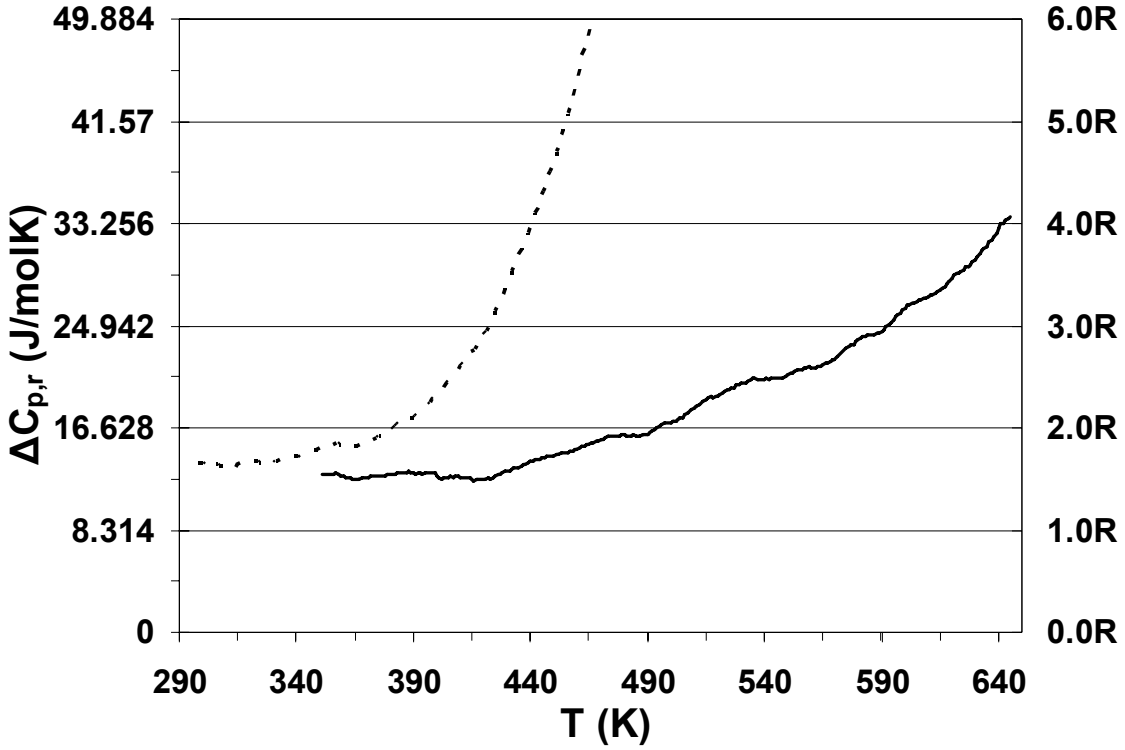

Figure 2-8. The heat capacity of hydration in analcime as a function of temperature. The dotted line depicts the results of $\Delta C_{p,r}$ derived from data collected in this study, and the solid line represents the $\Delta C_{p,r}$ calculated by C_p data of hydrated analcime from Johnson et al. (1982) and C_p data of dehydrated analcime from this study. R is the gas constant.

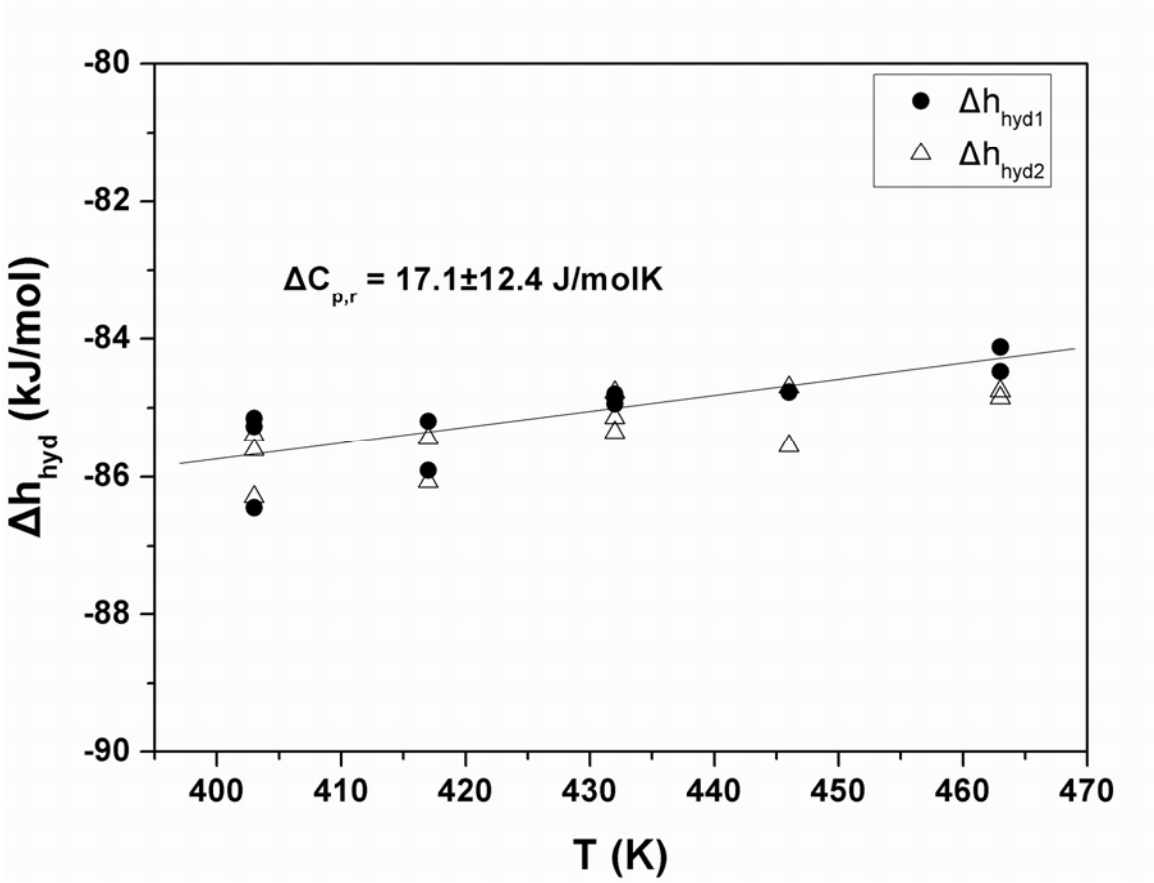

Figure 2-9. Partial molar enthalpies of hydration in analcime vs. temperature. The slope of the linear regression provides a magnitude for $\Delta C_{p,r}$.

CHAPTER 3
EXCESS HEAT CAPACITY IN NATROLITE HYDRATION

Introduction

Natrolite occurs in nature as an essentially stoichiometric mineral (composition $Na_2Al_2Si_3O_{10}\cdot 2H_2O$; Gottardi and Galli, 1985) and has one of the best-defined crystal structures of any zeolite, especially with respect to H_2O (in fact, it was the first zeolite structure refined; Pauling, 1930; Peacor, 1973; Artioli et al., 1984; Gottardi and Galli, 1985; Joswig and Baur, 1995). The framework of natrolite is composed of Si- and Al-centered tetrahedra. The arrangement of Si and Al in the tetrahedral sites is variable but tends to be largely ordered (e.g., Alberti et al., 1995; Neuhoff et al., 2002). Channels within the structure contain two Na^+ ions and two H_2O molecules per ten framework oxygens oriented in zigzag chains (Meier, 1960; Alberti and Vezzalini, 1981) (Fig. 3-1; Peacor, 1973). Each Na^+ ion is six coordinated to four framework oxygens and two H_2O molecules (Line and Kearley, 1998).

Natrolite occurs in a wide range of geologic environments, including soils (e.g., Ming and Allen, 2001), zeolite facies metabasites (Walker, 1960), and pegmatites around alkaline intrusions (e.g., Andersen et al., 1990). Despite the widespread occurrence of natrolite, its stability in geologic environments is poorly known. Previous studies mostly focused on the crystal structure (e.g., Peacor, 1973; Alberti et al., 1982; Joswig and Baur, 1995; Sapiga and Sergeev, 2001) and order/disorder (Si, Al) distribution (e.g., Alberti and Vezzalini, 1981; Hesse, 1983; Andersen et al., 1990; Ross et al., 1992; Neuhoff et al., 2002) of natrolite. Only a few works have explicitly considered the thermodynamic

stability of natrolite (e.g., Johnson et al., 1983; Vucelic and Vucelic, 1985; Paukov et al., 2002; Neuhoff and Keddy, 2004). Because natrolite occurs over a wide range of temperature and pressure, temperature (and pressure) dependent processes such as disordering and dehydration are important concerns in assessing the stability of this mineral. This is especially true because dehydration of natrolite leads to a large decrease in unit cell volume and a different space group (Peacor, 1973; Alberti and Vezzalini, 1983; Joswig and Baur, 1995; Baur and Joswig, 1996). After dehydration is complete, the rotation of the chains of Si and Al terahedra occurs simultaneously with the contraction of the lattice. Although natrolite can be completely rehydrated at low temperature, this process is complicated by the presence of hysteresis during cycled dehydration (heating) and rehydration (cooling). Unlike many zeolites, for which dehydration and rehydration are completely reversible, rehydration in natrolite, occurs at lower temperatures than does dehydration at a given chemical potential of water (van Reeuwijk, 1974).

The present study provides new insight into the thermodynamics of the dehydration process in natrolite. Heats of hydration as a function of temperature and the heat capacity of reaction are determined independently by differential scanning calorimetric (DSC) methods. Comparison of the results of these measurements reveals the existence of excess heat capacities and enthalpies of hydration, which in large part explain the cause of hysteresis in the dehydration behavior of this mineral.

Methods

Sample and Characterization

The sample of natrolite was previously described and characterized by Neuhoff et al. (2002; sample NAT001). It was collected as veins within a metabasaltic tectonic inclusion at the famous Dallas Gem Mine benitoite and neptunite locality, San Benito

County, California. Phase pure separates were hand picked, ground in an agate mortar, and sieved to a 20-40 μm size fraction. Sample identification and purity were confirmed by X-ray powder diffraction. The composition was determined by electron probe microanalysis at Stanford University to be essentially stoichiometric ($Na_2Al_2Si_3O_{10}{\cdot}nH_2O$). Water content of the sample was determined in this study by thermogravimetric heating to 1023 K after the equilibration with a room temperature atmosphere of 50 % relative humidity (RH). The mass loss is about 9.49% of total sample mass, very close to the ideal water content of natrolite (9.48%), and the water content taken to be 2 moles of water per formula unit.

Heat Capacity Measurements

The heat capacities of hydrated and dehydrated natrolite were determined by DSC with the Netzsch STA 449C Jupiter simultaneous DSC-thermogravimetric analysis (TGA) system at the University of Florida. Each experiment consisted of four separate runs: 1) determination of background and baseline by measurement of an empty crucible; 2) DSC measurement of a standard (sapphire); 3) scanning heating of hydrated natrolite and 4) scanning heating of dehydrated natrolite. A sample of approximately 27 mg was packed into a covered Pt-Rh crucible before step 3 and remained until completion of the experiment. Data were collected in the range of 298 to 733 K (higher temperatures cause an irreversible structure change for natrolite; Joswig and Baur, 1995) at a scanning rate of 15 K/min. A purge of dry N_2 was used during the experiment to keep the relative humidity below 1%, and the gas flow was maintained at ~30 ml/min using mass flow controllers. The furnace was heated to 733 K in each run and then cooled back to room temperature by liquid N_2 for next step. During heating, hydrated natrolite lost mass with increasing temperature and finally became completely dehydrated. The resulting

dehydrated natrolite was kept in an environment of dry N_2 to avoid rehydration during cooling to room temperature and then measured by scanning heating again. Heat capacity of the sample as a function of temperature was calculated by

$$C_p = \frac{m_{std}}{m_s} \times \frac{DSC_s - DSC_b}{DSC_{std} - DSC_b} \times C_{p,\,std} \tag{3-1}$$

where m_s is the mass of sample, m_{std} is the mass of standard (27.314 mg), DSC_s, DSC_{std} and DSC_b are for sample, standard and baseline respectively. Triplicate calorimetric measurements were conducted and averaged, and the error of the result is within 1% of the average value.

Absorption Calorimetry

Heats of hydration as a function of temperature were determined using an isothermal DSC-based immersion technique described by Neuhoff and Wang (2006). This approach combines the benefits of DSC and gas absorption calorimetry. Twenty to 30 mg of hydrated natrolite was placed into the Pt-Rh crucible for each run. The sample was dehydrated by scanning heating from 298 to 733 K at the rate of 15 K/min and then allowed to cool to the experimental temperature. A purge of dry N_2 was maintained at flow rate of 50 ml/min during this period. After equilibration (20-40 min) under dry gas at this temperature until both DSC and TGA baselines stabilized, the gas stream was changed to humid N_2 which was generated by bubbling N_2 through saturated NaCl solution. In order to reduce the change of DSC baseline, the flow rate of humid N_2 was maintained at 30 ml/min and the corresponding water vapor pressure in the furnace was ~12 mbar. Under this condition the sample was allowed to react until the DSC and TGA baselines stabilized again. Experiments were repeated on the same sample but indicated a

progressive loss of hydration capacity and decrease in hydration heat. Consequently, a fresh aliquot of sample was used for each experiment.

Results

Heat Capacities of Hydrated and Dehydrated Natrolite

The TGA and DSC traces of hydrated and dehydrated natrolite obtained during scanning heating are shown in Fig. 3-2. It can be seen that natrolite starts dehydrating at a relatively high temperature, ~450 K, and dehydration occurs over a fairly short range of temperature (450-673 K). The TGA trace also suggests that there is only one energetically distinct water site in natrolite, because the curve is continuous and does not show any inflections. In addition, only one peak is observed in the DSC and first derivative of TGA (dTGA) signals, consistent with this interpretation. The TGA curve of dehydrated natrolite shows no mass change during the scanning heating, which also indicates that the sample had been fully dehydrated in the first run and the condition for the experiment was dry enough to avoid rehydration of the sample.

Heat capacities of hydrated and dehydrated natrolite calculated from the DSC in Fig. 3-2b are shown in Table 3-1. Figure 3-3 depicts the C_p data of both hydrated and dehydrated natrolite determined by DSC data from the same experiment from 320 to 680 K. The heat capacity of dehydrated natrolite is relatively insensitive to the temperature. Calculated C_p for hydrated natrolite exhibits a strong positive inflection at ~450 K reflecting excess heat associated with dehydration of the sample.

Enthalpy of Hydration in Natrolite

An example of TGA and DSC response of natrolite during immersion in water vapor at 412 K is shown in Fig. 3-4. Note that after the atmosphere changed, but before the onset of rehydration, the DSC baseline does not change. The marked changes in both

TGA and DSC signal shortly after the atmosphere changed reflect absorption of water vapor by the sample. The mass of the sample increases as it absorbs more water, and the absorption rate is essentially constant for most of the reaction. Rehydration of natrolite is relatively rapid, with the whole process only taking about 110 minutes. Once hydration is complete, the baseline of TGA and DSC becomes stable again.

The heat flow of the natrolite hydration is proportional to the area under the DSC curve, which allows a calculation of the enthalpy of hydration (ΔH_{hyd}) by the equation:

$$\Delta H_{hyd} = -18.015A / km_{gain} \quad (3\text{-}2)$$

where A is the area under the DSC curve, m_{gain} is the mass gain in the rehydration and k is the caloric calibration factor. The results of ΔH_{hyd} for natrolite at four different temperatures are listed in Table 3-2 and shown in Fig. 3-5. The values of ΔH_{hyd} at the same temperature are very close (<0.5% difference), and the errors include the part from standard deviation of the values and that from the calorimetric calibration (1% of the results), which have been investigated to be within 1.5%.

It can be seen in Table 3-2 that the degree of rehydration mainly depends on the temperature. The masses of water absorbed during the rehydration at the same temperature are similar, except one at 412 K with a mass gain of about 9.34%, which may result from an abnormally higher water vapor pressure. Rehydrations of natrolite were also attempted at higher temperatures. Generally, the degree of rehydration increases with decreasing temperature below ~432 K, even though the difference between the mass gains during the rehydration at different temperatures is small (with only about 0.5% difference from 323 to 432 K). However, at temperatures above ~432 K the degree of rehydration decreases rapidly with increasing temperature. The fraction of water

absorbed during the rehydration drops by about 1.4% from 432 to 482 K. The sample of dehydrated natrolite can not rehydrate when the temperature reaches 522K (the fraction of water aborbed <0.1%). This behavior is also manifested by the mass change of natrolite in the scanning heating (with a heating/cooling rate of 5 K/min) dehydration-rehydration experiment (Fig. 3-6). The whole process is run under a humid condition with a constant water vapor pressure (~12 mbar). Note that the rehydration does not commence until the temperature decreases to about 513 K, similar to the results of the isothermal immersion experiments in which natrolite could not rehydrate above 522 K.

Discussion

Comparison with Previous Results

Johnson et al. (1983) have measured the C_p of natrolite from 5 to 350 K by adiabatic calorimetric method, and Drebushchak (1990) determined the C_p of dehydrated natrolite by DSC from room temperature to 800 K. In the present study we measured the C_p for both hydrated and dehydrated natrolite from 143 to 703 K, which covers some temperature ranges in the previous studies. The data presented here for hydrated and dehydrated natrolite are the average values of the results of three measurements starting from 143 K. These data are compared to previously published results in Fig. 3-7. It can be seen that the results of present study agree well with those of Johnson et al. (1983) and Drebushchak (1990). For instance, at 298.15 K C_p of hydrated natrolite measured in this study differs within 0.5% of that determined by Johnson et al. (1983), and the difference between the C_p of dehydrated natrolite in this study and that of Drebushchak (1990) is about 0.7%. However, C_p data for dehydrated natrolite in the present study exhibits a small peak near 500 K, indicating a small, reversible λ phase transition, that is not present in the data of Drebushchak (1990).

The various determinations of ΔH_{hyd} from the literature are listed in Table 3-2, and no correlations between ΔH_{hyd} and temperature can be observed from these values. Compared to these values, the result of ΔH_{hyd} at 451 K in this study agrees within error with that of Guliev *et al.* (1989) determined by immersion calorimetry at a similar temperature. In addition, the value of ΔH_{hyd} in this study increases with increasing temperature, showing that the hydration of natrolite becomes less energetic at higher temperatures, which is consistent with thermodynamic theory. According to the theory and the similar difference between the vaules of ΔH_{hyd} in this study, the ΔH_{hyd} at 298.15 K is interpreted to be similar to the one of Kiseleva *et al.* (1997) determined by transposed temperature drop calorimetry. The other values of ΔH_{hyd} for natrolite reported in the literature were determined at significantly different temperatures; however, all of the data are similar in magnitude (and mostly within error) of the results from this study.

Heat Capacity of Hydration in Natrolite

Hydration of natrolite can be represented by the reaction

$$\underset{\text{dehydrated natrolite}}{Na_2Al_2Si_3O_{10}} + 2\ H_2O_{vapor} = \underset{\text{natroltie}}{Na_2Al_2Si_3O_{10}\cdot 2H_2O} \qquad (3\text{-}3)$$

for which the standard heat capacity change ($\Delta C_{p,r}$) is given by

$$\Delta C_{p,r} = C_{p,nat} - C_{p,denat} - C_{p,steam} \qquad (3\text{-}4)$$

where $C_{p,nat}$ and $C_{p,denat}$ are the heat capacities of hydrated and dehydrated natrolite, respectively; $C_{p,steam}$ is the heat capacity of water vapor. The results of present study provide two independent means of assessing the magnitude of $\Delta C_{p,r}$. The first is by direct calculation from measured C_p for hydrated and dehydrated natrolite along with $C_{p,steam}$ (Robie and Hemingway, 1995). The second is by noting that the heat capacity is defined as the differential change in heat with respect to temperature

$$\Delta C_{p,r} = \left(\frac{\partial \Delta H_{hyd}}{\partial T}\right)_p \quad (3\text{-}5)$$

thus the first derivative of calculated values of ΔH_{hyd} with respect to temperature also provides a means of assessing $\Delta C_{p,r}$.

Values of $\Delta C_{p,r}$ consistent with the C_p results listed in Table 3-1 and shown in Fig. 3-3 are given in Table 3-1 and illustrated in Fig. 3-8. It can be seen that $\Delta C_{p,r}$ increases steadily from value of ~4 J/mol-H_2O/K at 298.15 K to ~16.2 J/mol-H_2O/K at 360 K. Above 360 K until the sample starts to dehydrate at about 420 K, $\Delta C_{p,r}$ is relatively constant.

The temperature dependence of $\Delta C_{p,r}$ between room temperature and 360 K is indicative of a phase transition occurring in this region. Similar transitions have been noted in water molecules in synthetic zeolites A and X (Vucelic and Vucelic, 1985; Basler and Lechert, 1972) in which water molecules appear to change their state of motion over a protracted range of temperature, similar to a glass transition. This behavior is in contrast to the relatively sharp, λ-type transitions observed in water molecules in laumontite (Neuhoff and Bird, 2001) and wairakite (Neuhoff and Keddy, 2004).

The relative temperature insensitivity of $\Delta C_{p,r}$ above 360 K is consistent with statistical-mechanical model of the behavior of confined water molecules. Carey (1993), following Barrer (1978) used statistical-mechanical reasoning to suggest that the difference in C_p between absorbed H_2O and the gas phase is caused by the loss of translational and rotational degrees of freedom to weak vibrational modes within the zeolite structure. Thus, the heat capacity of hydration in zeolites reflects the transition between translational/rotational and vibrational modes. With this model, the $\Delta C_{p,r}$ increases by 0.5 R for every vibrational mode gained by the absorbed species, up to a

maximum of 3R (Bish and Carey, 2001). The heat capacity of hydration for natrolite in our study is relatively insensitive to the temperature between 373 and 403 K, and the value is almost constant, ~16.24 J/mol-H_2O/K. According to the statistical-mechanical model, it is reasonable to suppose that the $\Delta C_{p,r}$ of hydration in natrolite is about 2R.

In contrast, the temperature dependence of ΔH_{hyd} data in Table 3-2 and Fig. 3-5 indicate a significantly higher value of $\Delta C_{p,r}$. Linear regression of these data indicates an average value of $\Delta C_{p,r} = 68.0 \pm 22.7$ J/mol-H_2O/K. This value is nearly four times the value determined by direct measurement of C_p for the phases in the reaction. Although the limited range of temperature and number of data points preclude rigorous analysis of the temperature dependence of $\Delta C_{p,r}$, the essentially linear trend of these data suggests that this property is relatively temperature-invariant over this temperature range. The discrepancy between $\Delta C_{p,r}$ determined directly from C_p measurements of individual phases and that assessed via equation 3-5 indicates that there is an excess contribution to C_p of mixing in this region. Such a contribution would not be detected in direct C_p measurements (and for reasons cited below can not be assessed for partially hydrated natrolite), further underscoring the need for direct measurements of heat capacities and enthalpies of hydration in zeolites. The presence of excess C_p of mixing in the solid solution between natrolite and dehydrated natrolite indicates that there must also be excess properties in the integral properties of C_p of mixing, namely the Gibbs energy, enthalpy, and entropy of mixing.

Nature of the Natrolite-Dehydrated Natrolite Solid Solution

The behavior of natrolite observed in this study suggests that the solid solution between its hydrated and dehydrated forms behaves in a fundamentally different fashion from that often observed in other zeolites. In many zeolites, dehydration is fully

reversible, with similar water content observed under identical conditions of temperature, pressure, and the chemical potential of H_2O during both dehydration and rehydration (e.g., Balgord and Roy, 1973; Carey and Bish, 1996; Fialips et al., 2005). In natrolite, however, it appears that significant hysteresis is observed between water contents achieved during hydration and dehydration. We suggest that this phenomenon is the result of solvus behavior of natrolite in this solid solution, which is consistent with the behavior of natrolite during rehydration as well as the energetics of natrolite hydration discussed above.

As shown in Fig. 3-6 that a strong hysteresis effect occurs after the dehydration of natrolite, dehydrated natrolite could not follow the dehydration path and the rehydration is initiated not until about 130 K below the end-point of dehydration. The strong hysteresis is partly due to the high heating/cooling rate (5 K/min), for instance, with a heating/cooling rate of 2 K/min the rehydration begins about 50 K below the end-point of dehydration. Neimark et al. (2000) modeled hysteresis in water absorption in nanopores as a solvus, and found that the hysteresis was related to the pore structure characterization of the material. However, even when the dehydrated natrolite starts absorbing water at about 513 K, the trace of mass change is still quite different from that of dehydration. The rehydration of natrolite should have reached equilibrium below 513 K as indicated by the isothermal immersion experiments. That means the hysteresis is probably present at equilibrium, and this is also supported by the evidence that limited degree of rehydration is possible above 473 K. Similar hysteretic phenomena were observed in the W1 site in laumontite (Fridriksson et al., 2003) and smectite (Tamura et al., 2000) that are clearly associated with the presence of two coexisting phases.

The rate of hydration in natrolite also shows a different feature from many other zeolites. The hydration rate of most zeolites depends on the degree of hydration (the concentration of reactant; e.g., analcime, Fig. 2-2). However, in natrolite the TGA signal increases monotonically during hydration until leveling off after reaction was complete (Neuhoff and Wang, 2006). Thus, the rate of hydration in natrolite is independent of the hydration degree, and the hydration of natrolite is a zero order reaction. This can be explained by the solvus behavior of natrolite. During the hydration of natrolite, two immiscible solutions (hydrated and dehydrated natrolite) coexist as a mechanical mixture, so the concentration of dehydrated natrolite remains constant during the whole process. The phenomena of hysteresis and zero order kinetics are not observed in many zeolites, such as chabazite (van Reeuwijk, 1974), mordenite, analcime and K-clinoptilolite (Bish and Carey, 2001), etc. Consequently, we believe that the special characters of hydration in natrolite (like excess heat capacity, hysteresis effect and zero order kinetics) are mainly attributed to the solvus behavior of natrolite in solid solution.

Table 3-1. Heat capacities of hydrated and dehydrated natrolite, steam, and hydration of natrolite at different temperatures.

T (K)	$C_{p, an}$ (J/molK)	$C_{p, dean}$ (J/molK)	$C_{p, H2O}$ (J/molK)	$\Delta C_{p, r}$ (J/mol-H_2O/K)
298.15	360.37	285.30	33.59	3.94
300	362.00	286.29	33.59	4.27
310	370.62	290.89	33.58	6.28
320	379.48	295.25	33.59	8.53
330	388.27	299.33	33.61	10.87
340	396.55	303.40	33.64	12.93
350	403.94	307.80	33.69	14.38
360	410.16	312.17	33.74	15.26
370	415.54	316.43	33.80	15.75
380	420.39	320.53	33.88	16.05
390	424.95	324.59	33.95	16.23
400	429.74	328.34	34.04	16.67
410	434.48	332.18	34.13	17.03
420	439.87	336.13	34.22	17.65
430	446.04	340.06	34.32	18.67
440	453.23	344.13	34.42	20.13

Table 3-2. Isothermal immersion calorimetric data for natrolite.

T (K)	Sample mass (mg)	Duration[1] (min)	Mass gain[2] (%)	ΔH_{hyd} (kJ/mol-H_2O)	$\Delta H_{hyd, ave}$[3] (kJ/mol-H_2O)	Error (kJ/mol-H_2O)
412	23.97	121	9.18	-97.16	-97.37	0.99
412	25.41	100	9.17	-97.50		
412	25.48	95	9.34	-97.44		
432	24.4	87	9.18	-95.74		
432	24.24	83	9.24	-95.49	-95.69	0.97
432	29.76	117	9.21	-95.84		
451	29.44	127	9.17	-94.70		
451	23.6	114	9.15	-94.55	-94.67	0.95
451	27.56	109	9.14	-94.77		
472	29.34	130	8.96	-93.21		
472	27.45	126	8.93	-93.21	-93.19	0.93
472	25.73	118	8.94	-93.16		

[1]Duration of immersion portion of experiment used in data regression. [2]Mass of the H_2O (in percentage) absorbed in that period. [3]The average value of ΔH_{hyd}, as the integral enthalpy of hydration in natrolite.

Table 3-3. Enthalpy of hydration in natrolite.

Composition	Method[1]	Temperature (K)	ΔH_{hyd} (kJ/mol-H_2O)
$(NaAl)_2Si_2O_{10}\cdot 2H_2O$	TTD	298.15	-101.7 ± 3.6[2]
$(NaAl)_2Si_2O_{10}\cdot 2H_2O$	PE	900	-108[3]
Not reported	PE	684.15	-102.9 ± 4.0[4]
Not reported	DSC	623.15	-89.1[5]
$(NaAl)_2Si_2O_{10}\cdot 2H_2O$	IM	453.15	-100.0 ± 5.0[6]

[1]Methods: TTD: transposed temperature drop calorimetry; PE: retrieval from phase equilibrium observations; DSC: calculated from scanning DSC measurement; IM: heat of immersion in water.
[2]Kiseleva et al. (1997)
[3]Hey (1932)
[4]van Reeuwijk (1974)
[5]van Reeuwijk (1972)
[6]Guliev et al. (1989)

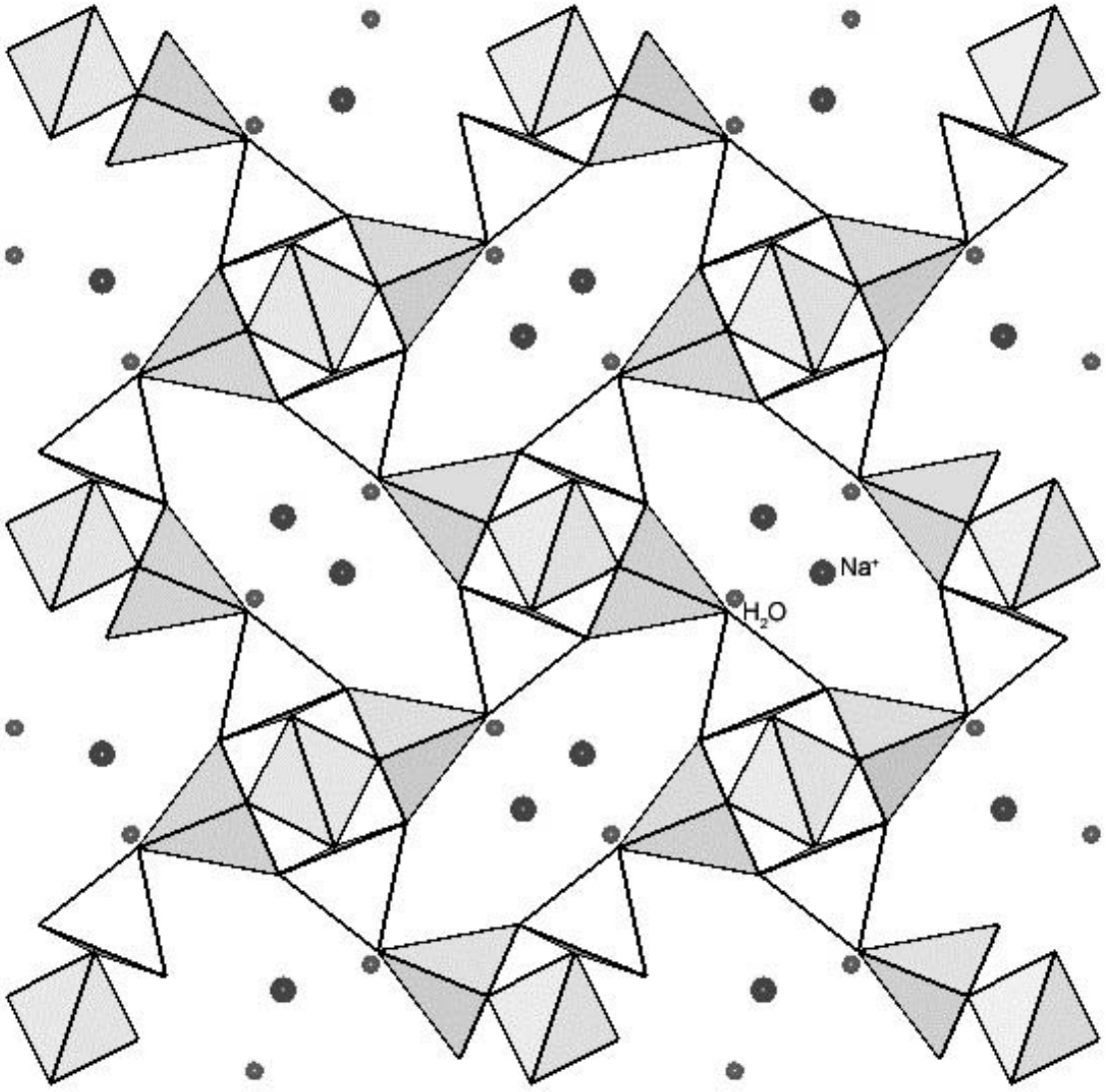

Figure 3-1. Crystal structures of natrolite down the *c* crystallographic axis. (after Peacor, 1973). The framework of Si- and Al- centered tetrahedra are surrounded by four oxygens. The big spheres denote the positions of Na^+ ions. The small spheres are the positions of water molecules.

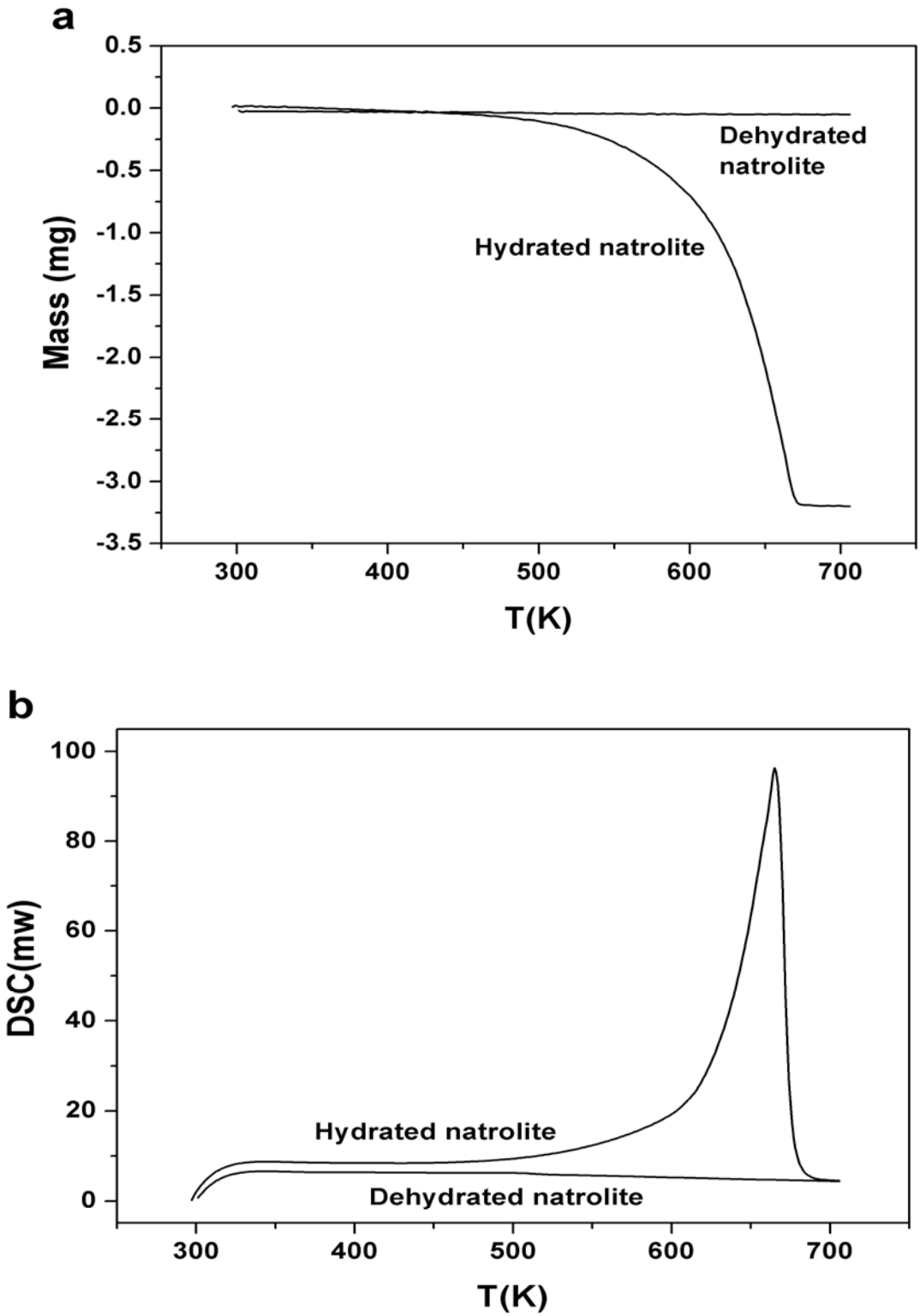

Figure 3-2. The mass change (a) and DSC response (b) of hydrated and dehydrated collected at a scanning rate of 15 K/min under ultrapure N_2.

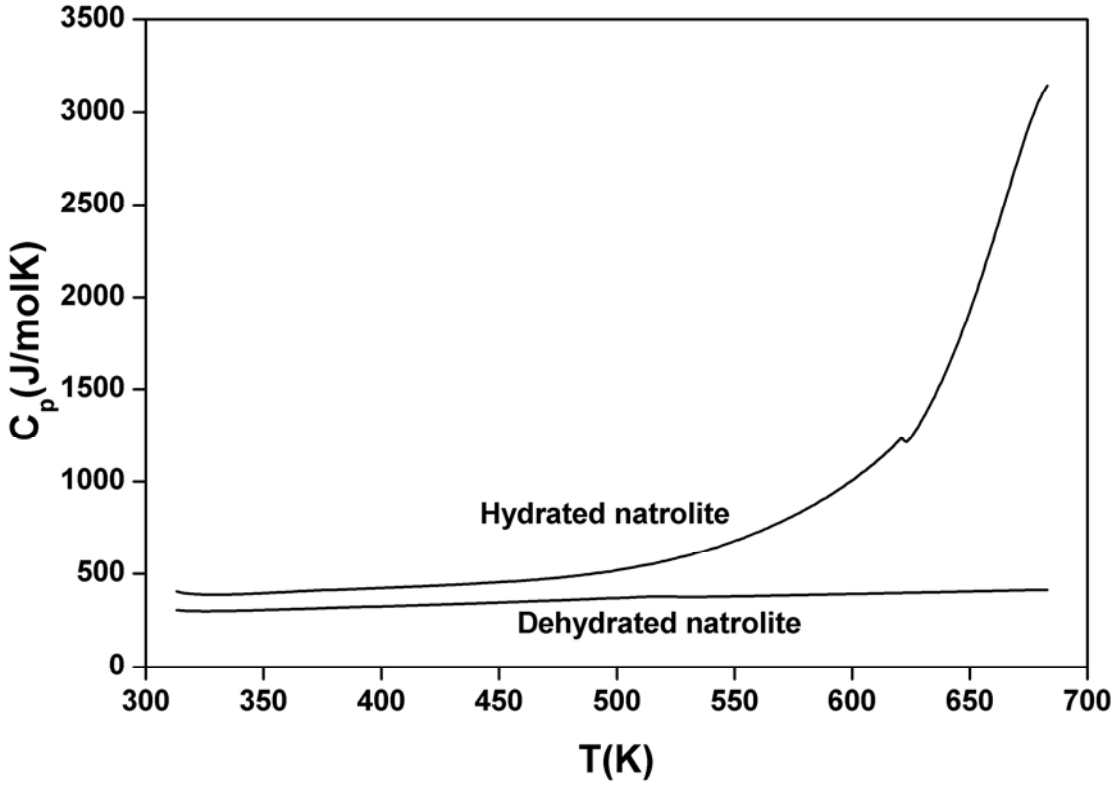

Figure 3-3. Heat capacities of hydrated and dehydrated natrolite as a function of temperature from 320 to 680 K, which are calculated from the DSC data collected in the same scanning heating experiment.

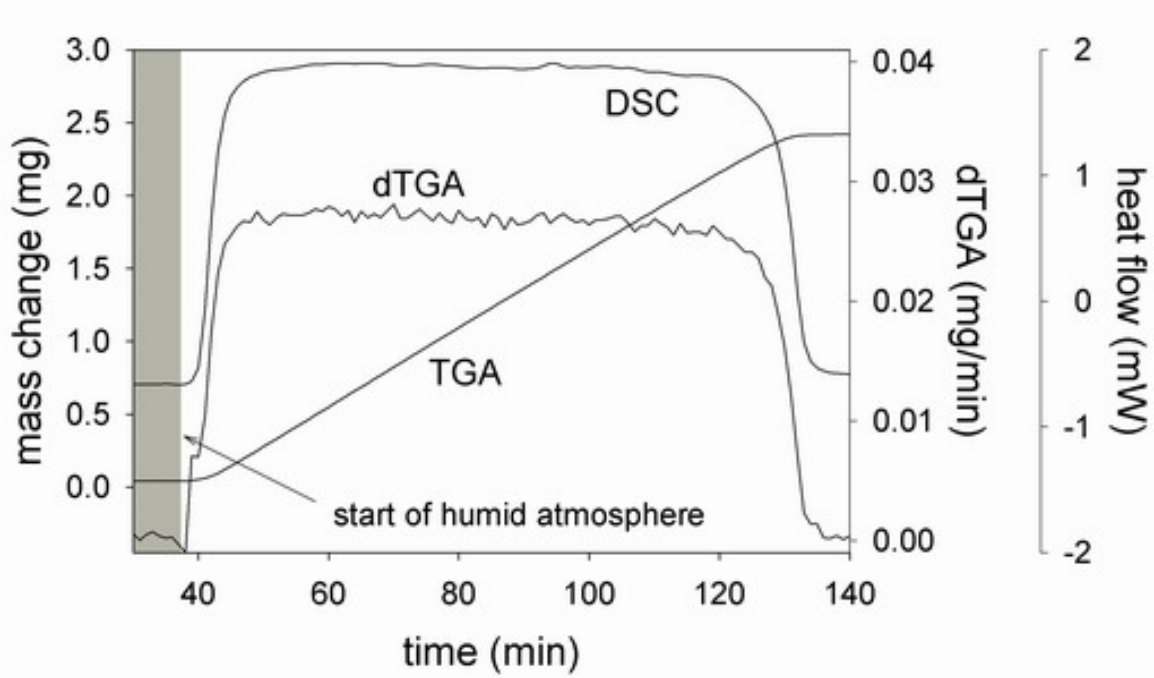

Figure 3-4. Example immersion calorimetric experiment on natrolite conducted at 412 K. Simultaneously-recorded TGA and DSC signals for natrolite as a function of temperature. The first derivative of the TG curve is given by the curve labeled dTGA. Region of the gray box denotes initial equilibration of sample at experimental temperature under dry N_2. The rest of the experiment was conducted in the presence of a flow of humidified N_2.

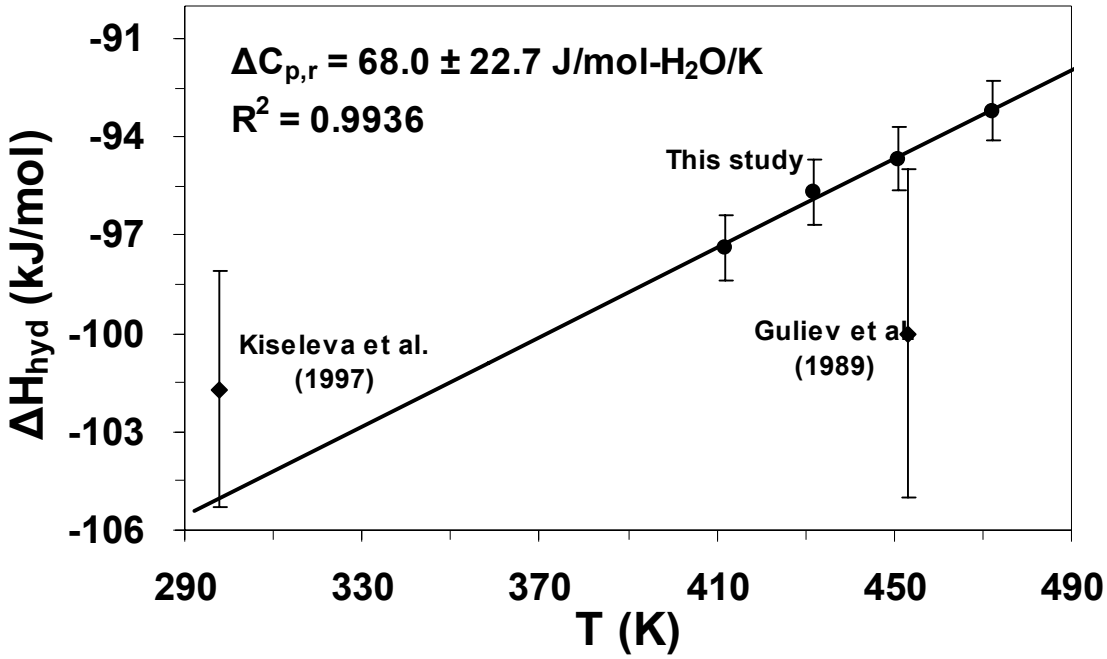

Figure 3-5. The enthalpy of dehydration in natrolite as a function of temperature. The slope of the linear regression is the value of $\Delta C_{p,r}$.

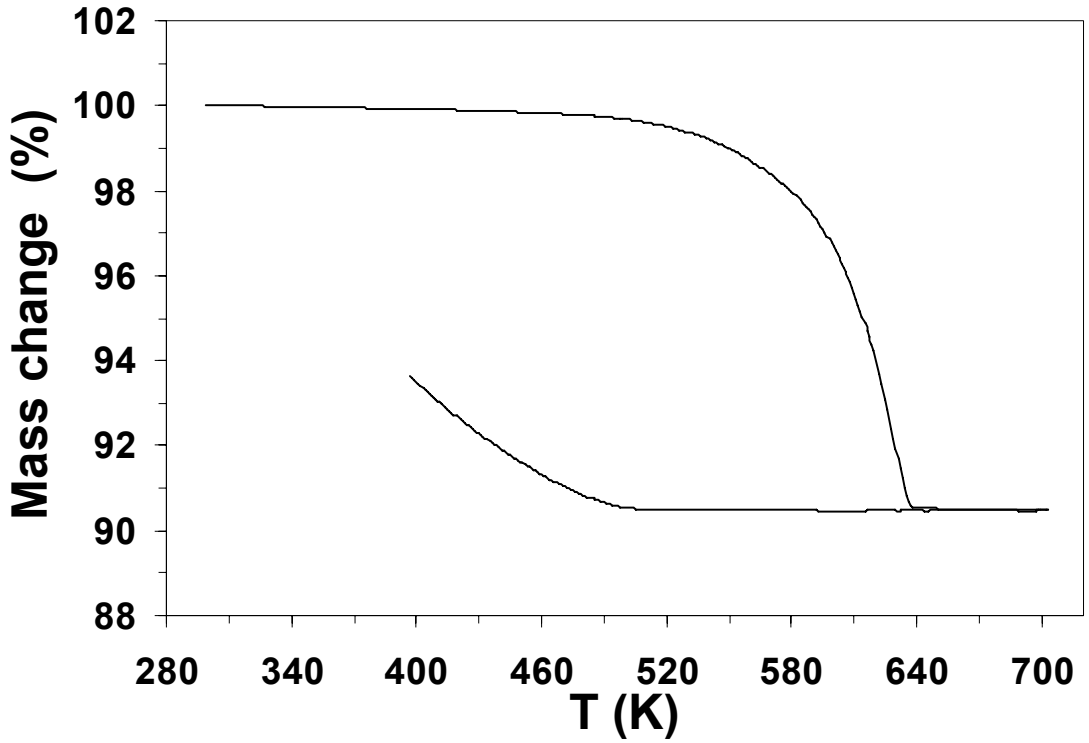

Figure 3-6. Mass change of natrolite in the dehydration and rehydration with a heating/cooling rate of 5 K/min under a humid condition (P_{H2O}≈12 mbar). A significant hysteresis occurs in the rehydration of natrolite.

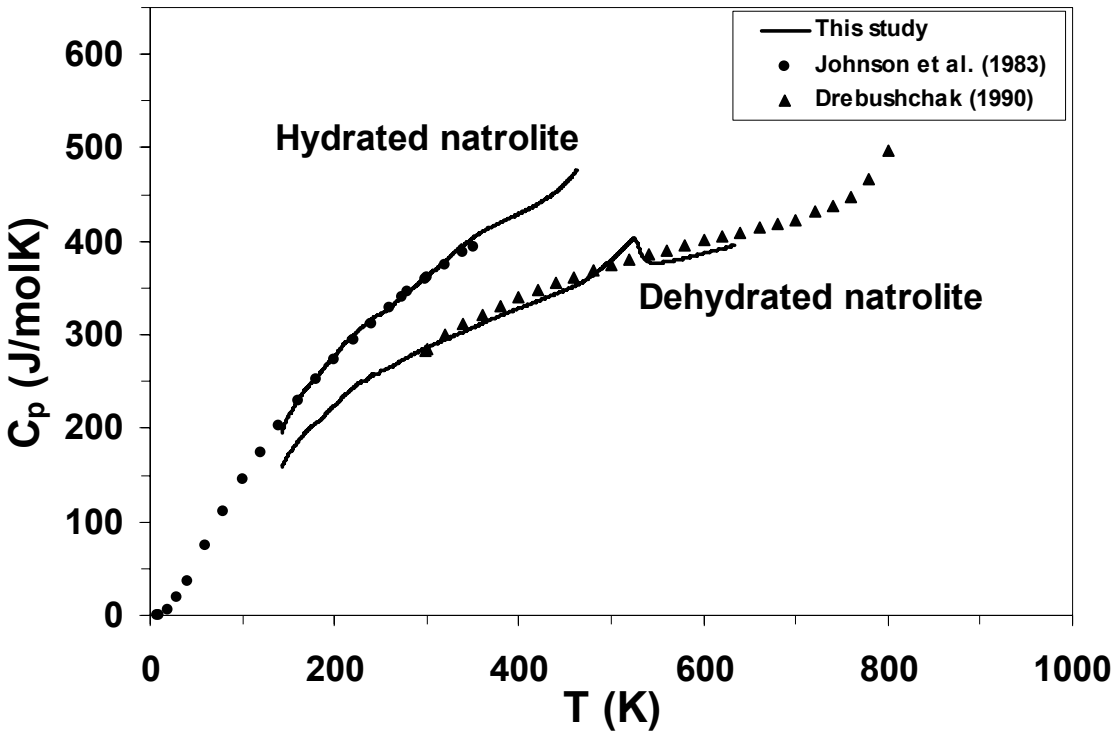

Figure 3-7. Comparison of present and previous C_p data for both hydrated and dehydrated natrolite. Our data are the average values of C_p from three different measurements starting from 143 K.

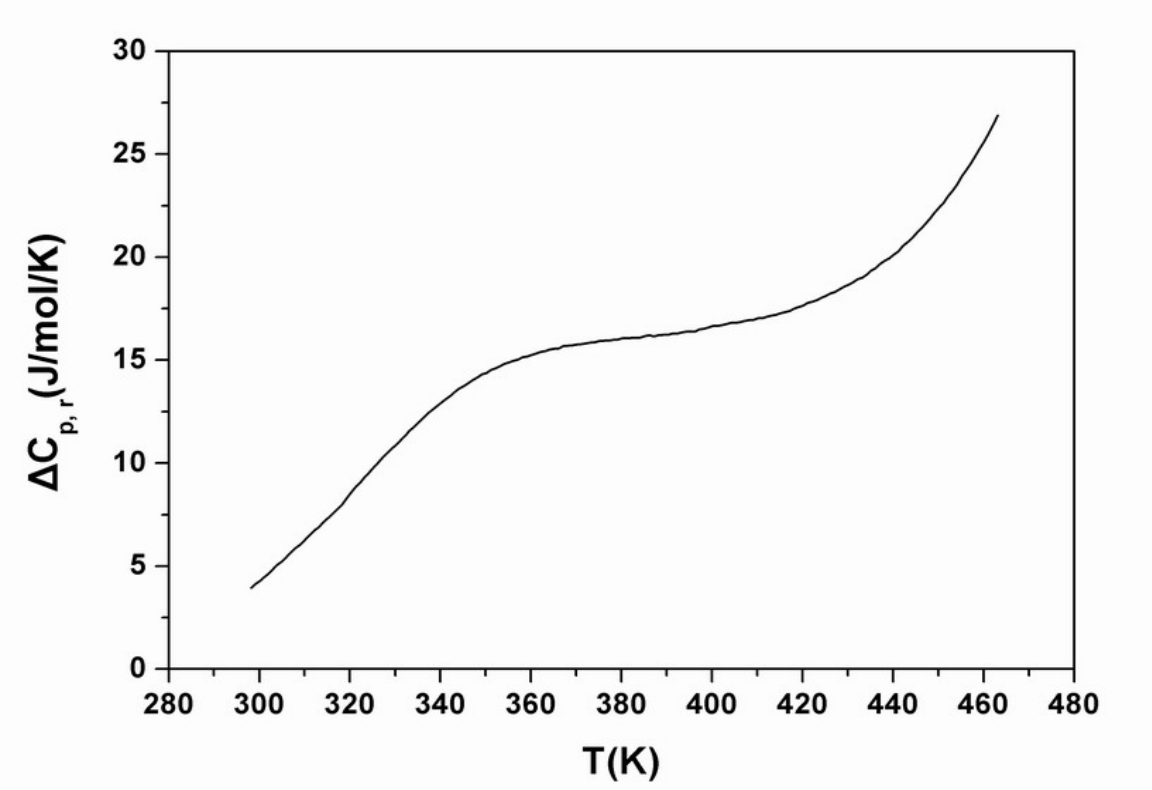

Figure 3-8. The heat capacity of hydration in natrolite as a function of temperature.

CHAPTER 4
CONCLUSION

Comparison of the Results of Analcime and Natrolite

Heat capacities of hydration directly measured by DSC technique for analcime and natrolite behave differently with increasing temperature. However, they both have a temperature range in which $\Delta C_{p,r}$ is relatively insensitive to the temperature, 298 to 430 K for analcime and 370 to 410 K for natrolite. The data in these ranges conform to the statistical-mechanical model which argues that $\Delta C_{p,r}$ is related to the weak vibrational modes for absorbed H_2O compared with rotational and translational freedom in the vapor-phase molecule and it is independent of temperature (Carey, 1993). However, enthalpies of hydration in analcime and natrolite determined by an isothermal DSC-based immersion technique at different temperatures illustrate two phenomena that complicate application of the statistical mechanical model for $\Delta C_{p,r}$. In natrolite, a linear relationship exists between ΔH_{hyd} and temperature, indicating a temperature independent $\Delta C_{p,r}$. However, the $\Delta C_{p,r}$ for natrolite hydration calculated by this approach is about 68.0 ± 22.7 J/molK, nearly four times the value determined by the model. A temperature independent excess heat capacity is suggested to exist in the hydration of natrolite. This excess heat capacity is probably related to the solvus behavior in the natrolite-dehydrated natrolite solid solution. In analcime, ΔH_{hyd} between 298 and 470 K is relatively insensitive to the temperature and implies a value of $\Delta C_{p,r}$ of approximately 2R. This result is consistent with that of the calorimetric $\Delta C_{p,r}$, showing the applicability of statistical-mechanical model for analcime in the relatively low temperature range.

However, the abrupt change of ΔH_{hyd} above 470 K suggests a phase transition which has a significant effect on $\Delta C_{p,r}$, and can even make the $\Delta C_{p,r}$ become negative.

The thermodynamics of dehydration and rehydration in rock-forming zeolites are different even for the simple-structure materials like analcime and natrolite. The behavior of $\Delta C_{p,r}$ is more complicated as a function of temperature than expected by the statistical-mechanical model. That model may be applicable for certain zeolites under some low temperature conditions (e.g., 298.15 K), but it is probably invalid for the zeolites containing phase transition during dehydration and rehydration. The enthalpy of hydration in zeolites determined by the isothermal immersion technique is critical for understanding these processes.

Heuristic Outcomes of This Study

This study generated two unparalleled datasets on the temperature dependence of the heat of hydration in zeolites that both complement existing data and enhance our understanding of this important geochemical process. The thermodynamic properties of the zeolites studied here provide a better understanding of the stability and reactivity of these materials in the earth's crust. In addition, this study also provides important data for assessing the reactivity of these minerals and for developing new industrial applications for them. For instance, the thermodynamics of ion exchange by zeolites (which are a critical process in radioactive waste disposal, wastewater treatment, and soil remediation; e.g., Kallo, 2001; Pabalan and Bertetti, 2001; Ming and Allen, 2001) is largely a function of the change in hydration state accompanying this process. This study also has a direct impact on the study of other hydrate minerals, especially hydrated nanomaterials. The methods and insights gained from this study can be used to develop new investigations of

the relationship between hydration/dehydration processes and nanophase stability in other mineral systems.

Future Work

There are still several problems left unresolved in this study, for example, the reason that lead to the phase transition in the hydration of analcime, the behavior of $\Delta C_{p,r}$ in the higher/lower range of temperature for analcime hydration, the real cause of the excess heat capacity for natrolite dehydration. More experiments will be done to get the specific data to address these problems. Future work will also include the thermodynamics of dehydration and rehydration on the complex zeolites like chabazite, wairakite etc. Furthermore, some geologic observations of the temperature and pressure conditions under which zeolites (e.g., analcime, natrolite) form in nature will be done to compare the results determined in the lab with these observations. This will be significant to the development of the techniques in our study.

LIST OF REFERENCES

Alberti, A., Cruciani, G. and Daura, I. (1995) Order-disorder in natrolite-group minerals. *European Journal of Mineralogy*, **7**, 501-508.

Alberti, A., Pongiluppi, D. and Vezzalini, G. (1982) The crystal-chemistry of natrolite, mesolite and scolecite. *Neues jahrbuch Fur Mineralogie-Abhandlungen*, **143**, 231-248.

Alberti, A., and Vezzalini, G. (1981) A partially disordered natrolite: Relationships between cell parameters and Si-Al distribution. *Acta Crystallographica*, **B37**, 781-788.

Alberti, A., and Vezzalini, G. (1983) How the structure of natrolite is modified through the heating-induced dehydration. *Neues jahrbuch Fur Mineralogie-Monatshefte*, **3**, 135-144.

Alberti, A., and Vezzalini, G. (1984) Topological changes in dehydrated zeolites: Breaking of T-O-T bridges. Pp. 834-841 in: *Proceedings of the 6th International Conference on Zeolites* (A. Bisio and D.H. Olson, editors). Butterworths, Guildford, U.K.

Andersen, E.K., Andersen, I.G.K. and PlougSorensen, G., (1990) Disorder in natrolites: structure determinations of three disordered natrolites and one lithium-exchanged disordered natrolite. *European Journal of Mineralogy*, **2**, 799-807.

Armbruster, T. (1993) Dehydfration mechanism of clinoptilolite and heulandite-single-crystal X-ray study of Na-poor, Ca-rich, K-rich, Mg-rich clinoptilolite at 100 K. *American Mineralogist*, **78**, 260-264.

Armbruster, T., and Gunter, M.E. (2001) Crystal structures of natural zeolites. Pp. 1-68 in: *Natural Zeolites: Occurrence, Properties, Applications* (D.L. Bish and D.W. Ming, editors). Reviews in Mineralogy and Geochemistry **45**, Mineralogical Society of America and Geochemical Society.

Armbruster, T., and Kohler, T. (1992) Re- and dehydration of laumontite: a single-crystal X-ray study at 100 K. *Neues Jahrbuch Fur Mineralogie Monatshefte*, **9**, 385-397.

Artioli, G., Smith, J.V. and Kvich, A. (1984) Neutron diffraction study of natrolite, $Na_2Al_2Si_3O_{10}{\cdot}2H_2O$, at 20 K. *Acta Crystallographica Section C-Crystal Structure Communications*, **40**, 1658-1662.

Artioli, G., and Ståhl, K. (1993) Fully hydrated laumontite-A structure study by flat-plate and capillary powder diffraction techniques. *Zeolites*, **13**, 249-255.

Baldar, N.A., and Whittig, L.D. (1968) Occurrence and synthesis of soil zeolites. *Soil Science Society of America Proceedings*, **32**, 235.

Balgord, W.D., and Roy, R. (1973) Crystal chemical relationships in the analcite family. II. Influence of temperature and P_{H2O} on structure. *Molecular Sieves*, **16**, 189-199.

Banfield, J.F., and Zhang, H. (2001) Nanocrystals in the environment. Pp. 1-59 in: *Nanoparticles and the environment* (J.F. Banfield and A. Navrotsky, editors). Reviews in Mineralogy and Geochemistry **44**, Mineralogical Society of America.

Barany, R. (1962) Heats and free energies of formation of some hydrated and anhydrous sodium- and calcium-aluminum silicates. *U.S. Bureau of Mines Report of Investigations*, 5900.

Barrer, R.M., and Cram, P.J. (1971) Heats of immersion of outgassed ion-exchanged zeolites. Pp. 105-131 in: *Molecular Sieve Zeolites-II*. Advances in Chemistry Series **102**, American Chemical Society, Washington, D.C.

Barrer, R.M. (1978) *Zeolites and clay minerals as sorbents and molecular sieves*. Academic Press, London, 497 pp.

Basler, W.D., and Lechert, H. (1972) Molar heat measurements on adsorbed water in zeolites linde-13-X. *Zeitschrift Fur Physikalische Chemie-Frankfurt*, **78**, 199-204.

Baur, W.H., and Joswig, W. (1996) The phases of natrolite occurring during dehydration and rehydration studied by single crystal X-ray diffraction methods between room temperature and 923 K. *Neues Jahrbuch Fur Mineralogie-Monatshefte*, **4**, 171-187.

Bish, D.L., Vaniman, D.T., Chipera, S.J. and Carey, J.W. (2003) The distribution of zeolites and their effect on the performance of a nuclear waste repository at Yucca Mountain, Nevada, U.S.A. *American Mineralogist*, **88**, 1889-1902.

Bish, D.L., and Carey, J.W. (2001) Thermal behavior of natural zeolites. Pp. 403–452 in: *Natural Zeolites: Occurrence, Properties, Applications* (D.L. Bish and D.W. Ming, editors). Reviews in Mineralogy and Geochemistry **45**, Mineralogical Society of America and Geochemical Society.

Boettinger, J.L., and Graham, R.C. (1995) Zeolite occurrence in soil environments: An updated review. Pp. 23-27 in: *Natural Zeolites '93: Occurrence, Properties, Use.* International Committee on Natural Zeolites, Brockport, New York.

Boles, J.R., and Coombs, D.S. (1977) Zeolite facies alteration of sandstones in southland Syncline, New Zealand. *American Journal of Science*, **277**, 982-1012.

Carey, J.W. (1993) The heat capacity of hydrous cordierite above 295 K. *Physics and Chemistry of Minerals*, **19**, 578-583.

Carey, J.W., and Bish, D.L. (1996), Equilibrium in the clinoptilolite-H_2O system. *American Mineralogist*, **81**, 952-962.

Carey, J.W., and Bish, D.L. (1997) Calorimetric measurement of the enthalpy of hydration of clinoptilolite. *Clays and Clay Minerals*, **45**, 814-825.

Coombs, D.S., Ellis, A.J., Fyfe, W.S. and Taylor, A.M. (1959) The zeolite facies, with comments on the interpretation of hydrothermal syntheses. *Geochimica et Cosmochimica Acta*, **17**, 53-107.

Coombs, D.S., and Whetten, J.T. (1967) Composition of analcime from sedimentary and burial metamorphic rocks. *Geological Society of American Bulletin*, **78**, 269-292.

Coughlan, B., and Carroll, W.M. (1976) Water in ion-exchanged L, A, X, and Y zeolites: A heat of immersion and thermogravimetric study. *Journal of the Chemical Society, Faraday Transactions I*, **72**, 2016-2030.

Cronstedt, A.F. (1756) Ron och beskrifning om en obekant bärg art, som kallas zeolites. *Kongl. Vetenskaps Acad. Handl. Stockholm*, **17**, 120-123.

Cruciani, G., Martucci, A., and Meneghini, C. (2003) Dehydration dynamics of epistilbite by in situ time resolved synhrotron powder diffraction. *European Journal of Mineralogy*, **15**, 257-266.

Drebushchak, V.A. (1990) Calorimetric studies on dehydrated zeolites: natrolite, heulandite, chabazite, and mordenite. *Geochemistry International*, **5**, 123-130.

Fialips, C.I., Carey, W.J., and Bish, D.L. (2005) Hydration-dehydration behavior and thermodynamics of chabazite. *Geochimica et Cosmochimica Acta*, **69**, 2293-2308.

Fridriksson, Th., Neuhoff, P.S. and Bird, D.K. (1999) Ion exchange equilibria between heulandite and geothermal fluids. *Geological Society of America Abstracts with Programs*, **31**, A27.

Fridriksson, Th., Carey, J.W., Bish, D.L., Neuhoff, P.S. and Bird, D.K. (2003) Hydrogen-bonded water in laumontite II: Experimental determination of site-specific thermodynamic properties of hydration of the W1 and W5 sites. *American Mineralogist*, **7**, 1060-1072.

Galindo Jr.C., Ming, D.W., Morgan, A. and Pickering, K. (2000) Use of Ca-saturated clinoptilolite for ammonium from NASA's advanced life support wastewater system. Pp. 363-371 in: *Natural Zeolites for the Third Millennium* (C. Colella and F.A. Mumpton, editors). De Frede Editore, Naples, Italy.

Gopal, R., Hollebone, B.R., Langford, C.H. and Shigeishi, R.A. (1982) The rates of solar energy storage and retrieval in a zeolite-water system. *Solar Energy*, **28**, 424-424.

Gottardi, G. (1989) The genesis of zeolites. *European Journal of Mineralogy*, **1**, 479-487.

Gottardi, G., and Galli, E. (1985) *Natural Zeolites*. Springer-Verlag, Berlin, 409 pp.

Grigorieva, L.V., Salata, O.V., Kolesnikov, V.G. and Malakhova, L.A. (1988) Effectiveness of the sorptive and coagulational removal of enteric bacteria and viruses from water. *Khim Teknol Vody*, **10**, 458-461.

Guliev, T.M., Isirikyan, A.A., Mirzai, D.I. and Serpinskii, V.V. (1989) Energy of rehydration of natrolite and scolecite. *Bulletin of the Academy of Sciences of the USSR Division of Chemical Scienc*e, **37**, 1308-1310.

Hay, R.L., and Moiola, R.J. (1963) Authigenic silicate minerals in Searles Lake, California. *Sedimenology*, **2**, 312-332.

Hay, R.L. (1966) Zeolites and zeolitic reactions in sedimentary rocks. *Geological Society of America Special Paper*, **85**, 130.

Hay, R.L., and Sheppard, R.A. (2001) Occurrences of zeolites in sedimentary rocks: An overview. Pp. 217-234 in: *Natural Zeolites: Occurrence, Properties, Applications* (D.L. Bish and D.W. Ming, editors). Reviews in Mineralogy and Geochemistry **45**, Mineralogical Society of America and Geochemical Society.

Helgeson, H.C., Delany, J.M., Nesbitt, H.W. and Bird, D.K. (1978) Summary and critique of the thermodynamic properties of rock-forming minerals. *American Journal of Science*, **278A**, 1-229.

Hesse, K.F. (1983) Refinement of a partially disordered natrolite, $Na_2Al_2Si_3O_{10}{\cdot}2H_2O$. *Zeitschrift Fur Kristallographite*, **163**, 69-74.

Hey, M.H. (1932) Studies on the zeolites. Part III. Natrolite and metanatrolite. *Mineralogical Magazine*, **23**, 243-289.

Höhne, G.W.H., Cammenga, H.K. and Eysel, W. (1990) The temperature calibration of scanning calorimeters. *Thermochimica Acta*, **160**, 1-12.

Iijima, A., and harada, K. (1968) Authigenic zeolites in zeolitic palagonite tuff on Oahu, Hawaii. *American Mineralogist*, **54**, 182-197.

Iijima, A. (2001) Zeolites in petroleum and natural gas reservoirs. *Reviews in Mineralogy & Geochemistry*, **45**, 347-402.

Johnson, G.K., Flotow, H.E., O'Hare, P.A.G. and Wise, W.S. (1982) Thermodynamic studies of zeolites: analcime and dehydrated analcime. *American Mineralogist*, **67**, 736-748.

Johnson, G.K., Flotow, H.E., O'Hare, P.A.G. and Wise, W.S. (1983) Thermodynamic studies of zeolites: Natrolite, msolite, and scolecite. *American Mineralogist*, **68**, 1134-1145.

Joswig, W., and Baur, W.H. (1995) The extreme collapse of a framework of NAT topology: the crystal structure of metanatrolite (dehydrated natrolite) at 548 K. *Neues jahrbuch Fur Mineralogie-Monatshefte*, **1**, 26-38.

Kallo, D. (2001) Applications of natural zeolites in water and wastewater treatment. Pp. 519-550 in: *Natural Zeolites: Occurrence, Properties, Applications* (D.L. Bish and D.W. Ming, editors). Reviews in Mineralogy and Geochemistry **45**, Mineralogical Society of America and Geochemical Society.

King, E.G. (1955) Low temperature heat capacity and entropy at 298.16 K of analcite. *Journal of the American Chemical Society*, **77**, 2192.

King, E.G., and Weller, W.W. (1961) Low temperature heat capacity and entropy at 298.15 K of some sodium- and calcium-aluminum silicates. *U.S. Bureau of Mines Report of Investigations*, 5855.

Kiseleva, I., Navrotsky, A., Belitsky, I.A. and Fursenko, B.A. (1996) Thermochemistry of natural potassium sodium calcium leonhardite and its cation exchanged forms. *American Mineralogist*, **81**, 668-675.

Kiseleva, I.A., Ogorodova, L.P., Melchakova, L.V., Belitsky, I.A. and Fursenko, B.A. (1997) Thermochemical investigation of natural fibrous zeolites. *European Journal of Mineralogy*, **9**, 327-332.

Kristmannsdóttir, H., and Tómasson, J. (1978) Zeolite zones in geothermal areas of Iceland. Pp. 277 –284 in: *Natural Zeolite Occurrence, Properties and Use* (L.B. Sand and F.M. Mumpton, editors). Pergamon Press, Oxford, UK.

Line, C.M.B., and Kearley, G.J. (1998) The librational and vibrational spectra of water in natrolite, $Na_2Al_2Si_3O_{10}{\cdot}2H_2O$ compared with abinitio calculations. *Chemical Physics*, **234**, 207–222.

Mazzi, F., and Galli, E. (1978) Is each analcime different. *American Mineralogist*, **63**, 448-460.

McCulloh T.H., Cashman S.H. and Stewart R.J. (1973) Diagnetic baselines for interpretive reconstructions of maximum burial depths and paleotemperatures in clastic sedimentary rocks. Pp. 18-46 in: *A Symposium in Geochemistry: Low Temperature Metamorphism of Kerogen and Clay Minerals*. Pacific Sect SEPM, Los Angeles.

McCulloh T.H., and Stewart R.J. (1979) Subsurface laumontite crystallization and porosity destruction in Neogene sedimentary basins. *Geological Society of America Abstracts with Programs*, **11**, 475.

Meier, W.M. (1960) The crystal structure of natrolite. *Z Kristallogr*, **113**, 430-444.

Meier, W.M., Olson, D. and Baerlocher, C. (2001) *Atlas of zeolite structure types*. Elsevier, Amsterdam, 302 pp.

Ming, D.W. (1985) Chemical and crystalline properties of clinoptilolite in South Texas soils. PhD dissertation, Texas A&M University, College Station, Texas, 257 pp.

Ming, D.W. (1987) Quantitative determination of clinoptilolite in soils by a cation-exchange capacity method. *Clays & Clay Minerals*, **35**, 463-468.

Ming, D.W. (1988) Occurrence and weathering of zeolites in soil environments. Pp. 699-715 in: *Occurrence, Properties, and Utilization of Natural Zeolites* (D. Kalló and H.S. Sherry, editors). Akadémiai Kiadó, Budapest, Hungary.

Ming, D.W., and Allen, E.R. (2001) Use of natural zeolites in agronomy, horticulture and environmental soil remediation. Pp. 619-654 in: *Natural Zeolites: Occurrence, Properties, Applications* (D.L. Bish and D.W. Ming, editors). Reviews in Mineralogy and Geochemistry **45**, Mineralogical Society of America and Geochemical Society.

Ming, D.W., and Mumpton, F.A. (1989) Zeolites in soils. Pp. 873-911 in: *Minerals in Soil Environments* (J.B. Dixon and S.B. Weed, editors). Soil Science Society of America, Madison, Wisconsin.

Muller, J.C.M., Hakvoort, G. and Jansen, J.C. (1998) DSC and TG study of water adsorption and desorption on zeolite NaA-Powder and attached as a layer on metal. *Journal of Thermal Analysis and Calorimetry*, **53**, 449-466.

Mumpton, F.A. (1977) Utilization of natural zeolites. Pp. 177-204 in: *Mineralogy and Geology of Natural Zeolites* (F.A. Mumpton, editor). Reviews in Mineralogy **4**, Mineralogical Society of America.

Navrotsky, A., Rapp, R.P., Smelik, E., Burnley, P., Circone, S., Chai, L., Bose, K. and Westrich, H.R. (1994) The behavior of H_2O and CO_2 in high-temperature lead borate solution calorimetry of volatile-bearing phases. *American Mineralogist*, **79**, 1099-1109.

Neimark, A.V., Ravikovitch, P.I. and Vishnyakov, A. (2000) Adsorption hysteresis in nanopores. *Physical Review E*, **62**, R1493-R1496.

Neuhoff, P.S., and Bird, D.K. (2001) Partial dehydration of lamontite: Thermodynamic constraints and petrogenetic implications. *Mineralogical Magazine*, **65**, 59-70.

Neuhoff, P.S., Fridriksson, Th. and Bird, D.K. (2000) Zeolite parageneses in the North Atlantic igneous province: Implications for geotectonics and groundwater quality of basaltic crust. *International Geology Review*, **42**, 15-44.

Neuhoff, P.S., Hovis, G., Balassone, G. and Stebbins, J. (2004) Thermodynamic properties of analcime solid solutions. *American Journal of Science*, **304**, 21-65.

Neuhoff, P.S., and Keddy, S.M. (2004) Heat capacity of intra-crystalline water molecules in zeolites. *Geological Society of America Abstracts with Programs*, **36**, 260.

Neuhoff, P.S., Kroeker, S., Du, L., Fridriksson, Th. And Stebbins, J. (2002) Order/disorder in natrolite group zeolites: A 29Si and 27Al MAS NMR study. *American Mineralogist*, **87**, 1307-1320.

Neuhoff, P.S., Stebbins, J.F. and Bird, D.K. (2003) Si-Al disorder and solid solutions in analcime, chabazite and wairakite. *American Mineralogist*, **88**, 410-423.

Neuhoff, P.S., and Wang, J. (2006) Isothermal measurement of heats of hydration in zeolites by simultaneous thermogravimetry and differential scanning calorimetry. Submitted to *Clays and Clay Minerals*.

Neuhoff, P.S., Watt, W.S., Bird, D.K. and Pedersen, A.K. (1997) Timing and structural relations of Regional Zeolite Zones in Basalts of the East Greenland continental Margin. *Geology*, **25**, 803-806.

Neveu, A., Gaspard, M., Blanchard, G., and Martin, G. (1985) Intracrystalline self-diffusion of ions in clinoptilolite ammonia and sodium-cations studies. *Water Research*, **19**, 611-618.

Newell, P.A., and Rees, L.V.C. (1983) Ion-exchange and cation site locations in zeolite L. *Zeolites*, **3**, 22-27.

Ogorodova, L.P., Kiseleva, I.A., Mel.chakova, L.V., Belitskii, I.A. and Fursenko, B.A. (1996) Enthalpies of formation and dehydration of natural analcime. *Geochemistry International*, **34**, 980-984.

Pabalan, R.T., and Bertetti, E.P. (1999) Experimental and modeling study of ion exchange between aqueous solutions and the zeolite mineral clinoptilolite. *Journal of Solution Chemistry*, **28**, 367-393.

Pabalan, R.T., and Bertetti, E.P. (2001) Cation-exchange properties of natural zeolties. Pp. 453-518 in: *Natural Zeolites: Occurrence, Properties, Applications* (D.L. Bish and D.W. Ming, editors). Reviews in Mineralogy and Geochemistry **45**, Mineralogical Society of America and Geochemical Society.

Passaglia, E., and Sheppard, R.A. (2001) The crystal chemistry of zeolites. Pp. 69–116 in: *Natural Zeolites: Occurrence, Properties, Applications* (D.L. Bish and D.W. Ming, editors). Reviews in Mineralogy and Geochemistry **45**, Mineralogical Society of America and Geochemical Society.

Pankratz, L.B. (1968) High temperature heat contents and entropies of dehydrated analcite, kaliophilite, and leucite. *U.S. Bureau of Mines Report of Investigations*, 7073.

Paukov, I.E., Kovalevskaya, Y.A., Seretkin, Y.V. and Belitskii, I.A. (2002) The thermodynamic properties and structure of potassium-substituted natrolite in the phase transition region. *Russian Journal of Physical Chemistry*, **76**, 1406-1410.

Pauling, L. (1930) The structure of some sodium and calcium aluminosilicates. *Procedings of the National Academy of Sciences*, **16**, 453.

Peacor, D.R. (1973) High-temperature, single-crystal X-ray study of natrolite. *American Mineralogist*, **58**, 676-680.

Petrova, N., Mizota, T. and Fujiwara, K. (2001) Hydration heats of zeolites for evaluation of heat exchangers. *Journal of Thermal Analysis and Calorimetry*, **64**, 157-166.

Ransom, B., and Helgeson, H.C. (1994) Estimation of the standard molal heat capacities, entropies, and volumes of 2:1 clay minerals. *Geochimica et Cosmochimica Acta*, **58**, 4537-4547.

Ross, M., Flohr, M.J.K. and Ross, D.R. (1992) Crystalline solution series and order-disorder within the natrolite. *American Mineralogist*, **77**, 685-703.

Robie, R.A., and Hemingway, B.S. (1995) Thermodynamic properties of minerals and related substances at 298.15 K and 1 bar (105 pascals) pressure and at higher temperatures. *United States Geological Survey Bulleti*n, **2131**, 461.

Robie, R.A., Hemingway, B.S. and Fisher, J.R. (1979) Thermodynamic properties of minerals and related substances at 298.15 K and 1 bar (105 Pascals) pressure and at higher temperatures. *U.S. Geological Survey Bulletin*, **1452**, 456.

Sabbah, R., Xu-wu, A., Chickos, J.S., Planas Leitão, M.L., Roux, M.V. and Torres, L.A. (1999) Reference materials for calorimetry and differential thermal analysis. *Thermochimica Acta*, **331**, 93-204.

Sapiga, A.V., and Sergeev, N.A. (2001) NMR investigation of natrolite structure. *Crystal Research and Technology*, **36**, 875-883.

Sarge, S.M., Gmelin, E., Höhne, G.W.H., Cammenga, H.K., Hemminger, W. and Eysel, W. (1994) The caloric calibration of scanning calorimeters. *Thermochimica Acta*, **247**, 129-168.

Scarmozzino, R., Aiello, R. and Santucci, A. (1980) Chabazitic tuff for thermal storage. *Solar Energy*, **24**, 415-416.

Selvidge, M., and Miaoulis, I.N. (1990) Evaluation of reversible hydration reactions for use in thermal energy storage. *Solar Energy*, **44**, 173-178.

Shigeishi, R.A., Langford C.H. and Holleborne B.R. (1979) Solar energy storage using chemical potential changes associated with drying of zeolites. *Solar Energy*, **23**, 489-495.

Shim, S.H., Navrotsky, A., Gaffney, T.R. and Macdougall, J.E. (1999) Chabazite: Energetics of hydration, enthalpy of formation and effect of cations on stability. *American Mineralogist*, **84**, 1870-1822.

Stoiber, R.E., and Davidson, E.S. (1959) Amygdule mineral zoning in the Portage Lake Lava Series, Michigan Copper District. *Econoomic Geology*, **54**, 1250-1277.

Surdam, R.C., and Sheppard, R.A. (1978) Zeolites in saline, alkaline-lake deposits. Pp. 145-174 in: *Natural Zeolites: Occurrence, Properties, Use* (L.B. Sand and F.A. Mumpton, editors). Pergamon Press, Elmsford, New York.

Tamura, K., Yamada, H. and Nakazawa, H. (2000) Stepwise hydration of high-quality synthetic smectite with various cations. *Clays and Clay Minerals*, **48**, 400-404.

Thompson, A.B. (1973) Analcime: Free energy from hydrothermal data. Implications for phase equilibria and thermodynamic quantities for phases in $NaAlO_2$-SiO_2-H_2O. *American Mineralogist*, **58**, 277-286

van Reeuwijk, L.P. (1972) High-temperature phases of zeolites of the natrolite group. *American Mineralogist*, **57**, 499-510.

van Reeuwijk, L.P. (1974) The thermal dehydration of natural zeolites. Dissertation, Wageningen, Netherlands, 88 pp.

Vucelic, V., and Vucelic, D (1985) Heat capacities of water on zeolites. Pp. 475-480 in: *Zeolites* (B. Drzaj, S. Hocevar and S. Pejovnik, Editors). Elsevier, Amsterdam.

Walker, G.P.L. (1960) Zeolite zones and dike distribution in relation to the structure of basalts of eastern Iceland. *Journal of Geology*, **68**, 515-528.

Wilkin, R.T., and Barnes, H.L. (1999) Thermodynamics of hydration of Na- and K-clinoptilolite to 300 °C. *Physics and Chemistry of Minerals*, **26**, 468-476.

Wilkinson, J.F.G., and Hensel, H.D. (1994) Nephelines and analcimes in some alkaline igneous rocks. *Contributions to Mineralogy and Petrology*, **118**, 79-91.

Xu, G. (1990) Use of natural zeolite for ammonia in distilled water production. *Shuichuji Jishu*, **16**, 456-499.

BIOGRAPHICAL SKETCH

Jie Wang was born in Ezhou, Hubei Province, China, in January 1981. He lived in with his parents and attended elementary and high schools in that small town until entering the University of Science & Technology of China in 1999. He graduated with a B.S. in earth and space sciences in 2004. In August of 2004 he entered the University of Florida and continued his graduate study in the Department of Geological Sciences. He worked under Dr. Philip Neuhoff's direction and studied the thermodynamics of dehydration and rehydration in zeolites. Upon completion of master's study, he will keep on working with Dr. Neuhoff for his Ph.D. degree.